FABRICATION AND MECHANICAL ANALYSIS OF POLYMER-NANOCOMPOSITE MONOFILAMENTS

A THESIS SUBMITTED TO THE GRADUATE DIVISION OF THE UNIVERSITY OF HAWAI'I IN PARTIAL FULFILLMENT OF THE REQUIREMENTS FOR THE DEGREE OF

MASTER OF SCIENCE

IN

MECHANICAL ENGINEERING

MAY 2008

By
Garret Minoru Hashiro

Thesis Committee:

Anyuan Cao, Chairperson
Mehrdad Ghasemi-Nejhad
Ronald Knapp

We certify that we have read this thesis and that, in our opinion, it is satisfactory in scope and quality as a thesis for the degree of Master of Science in Mechanical Engineering.

THESIS COMMITTEE

Chairperson

ACKNOWLEDGEMENTS

First and foremost, I'd like to thank my advisor and mentor Dr. Anyuan Cao for introducing me to this cutting-edge field full of promise and potential in solving some of humanity's greatest obstacles. His unfailing guidance, generosity, and support through the past three years are what got me through the tough times. It's an honor to be one of his first graduate students. I'd also like to acknowledge Dr. Mehrdad N. Ghasemi Nejhad for overseeing the laboratory and providing support which made my graduate studies possible and Dr. Ronald Knapp for his time and generosity in providing assistance with the testing, as well as providing the inspiration for this research endeavor.

I'm forever grateful to my lab mates at the Hawai'i Nanotechnology Laboratory for making the endless hours spent in the lab all the more enjoyable; Davood Askari, Jess Kaneshiro, Vamshi Gudapati, Phillip Stuckey, Xianglong Li, and Vinod Veedu. Sincere thanks to Dr. Xianglong Li for his expertise and incredible support throughout this research. Thanks to Stuart Akagi, who I could always count on for help on the Instron testing and in the machine shop. I am also grateful to Tina Carvalho for training, assisting, and allowing me to use the SEM facility at the Biological Electron Microscope Facility. As well as, Dr. Lloyd Hihara who also provided SEM assistance.

I would like to acknowledge the assistance of the support staff in the Mechanical Engineering Department who made my work easier and enjoyable. Their procurement of the necessary research materials and aid logistically made all the difference in the world. To my Hawaiian language instructor Kaluhialoha Eldridge for helping me translate the abstract into Hawaiian. *E ho'okū'ono'ono ka mo'omeheu Hawai'i, ke akeakamai a me ka 'enehana kekahi i kekahi me ka lōkahi;* may the Hawaiian culture, science and technology prosper together in unity.

I am forever grateful to the College of Engineering which has been apart of my life for the past eight years, through my undergraduate study in the Civil Engineering Department. As well as, the school affiliated clubs-ASCE, Chi Epsilon, ASME, and SAE-which have provided me with countless of fond memories through the years.

To my friends and family who have put up with me and supported me throughout these years, thank you so very much. I am especially grateful to the support of my parents, Glenn and Linda Hashiro, who are just as excited for me as I finally embark on getting a real job. And to my little sister, Sheri, who provided the friendly sibling rivalry, good luck as you finish your graduate studies.

ABSTRACT

This is a systematic study of several key factors (e.g. materials, functionalization, dispersion, and concentration) and their influence on the mechanical properties of nanocomposites. A simple hot-pultrusion method was developed to continuously draw low-density polyethylene nanomaterial threads with lengths of the order of meters and micron range diameters. Mechanical properties such as ultimate strength, stiffness, strain to failure, and toughness were tested. Specifically, materials such as carbon nanotubes and cadmium sulfide nanoparticles were investigated at various concentrations. The effect of chemical functionalization was explored and compared with pristine samples. Data results revealed the degrading effects of the processing method as compared to the unprocessed control sample. However, compared to a secondary control sample which underwent the same processing method, the nanocomposites exhibited an improvement in material properties proportional to nanomaterial concentration. The results are expected to provide insight on the interaction between both 1-dimensional and 0-dimensional nanoscale fillers and polymers.

MO‘OLELO I HO‘OPŌKOLE ‘IA

(Hawaiian translation of abstract)

He noi‘ina kēia o kekahi mau mea nui (memea, *functionalization*, ho‘ohehe‘e, a me ka nui o ka memea). Ua noi‘ina ‘ia ka ho‘ololi ‘ana o nā mea nui i nā ‘ano kūmikini o nā memea. Ua ho‘omōhala au i kekahi ‘ano hana ma‘alahi e huki mau i nā lopi *low-density polyethylene nanocomposite*. Kīlepa nā lō‘ihi nā lopi. Loa‘a i nā lopi nā anawaena maikolona. Ua ho‘okolohua au i nā ‘ano kūmikini o nā memea (*ultimate strength, stiffness, strain to failure, and toughness*). Ua noi‘ina au i nā memea (*carbon nanotubes, cadmium sulfide nanoparticles)* i nā nui o nā memea nui like‘ole. Ua noi‘ina au i ka hopena o ka *functionalization* kemikala a ua ho‘ohālikelike i nā la‘ana ma‘ema‘e. Ua hō‘ike ‘ia nā hopena ‘ino o ka hana ‘ana ma o nā hopena, ke ho‘ohālikelike ‘ia me nā la‘ana kumu kūlohelohe. Na‘e, ua hō‘ike nā *nanocomposites* i ka ho‘omaika‘i ‘ana i nā ‘ano kūmikini o nā memea, ke ho‘ohālikelike ‘ia me ka lua o nā la‘ana kumu. Ua lākiō like ka ho‘omaika‘i ‘ana i ka *nanomaterial*. E ho‘olako ana ka hopena i ka na‘auao o ka pilina ma waena o nā mea ho‘opihapiha *nanoscale* a me nā *polymers*.

TABLE OF CONTENTS

LIST OF TABLES

LIST OF FIGURES

CHAPTER 1

INTRODUCTION

The onset of nanotechnology opened new doors for many scientific fields, particularly composite materials. Utilizing the extraordinary properties of nanomaterials, researchers have been studying their incorporation into various polymers. These polymer matrices adopt the characteristics of their nanomaterials to create new multi-functional composite materials [1-16]. These so-called "nanocomposites" will aid in the development of nano-sized electrical and mechanical systems, including sensors and other smart materials, as well as extraordinary strong building components for structural, automotive, aerospace, even ballistic purposes [17-23]. Other studies into polymer nanocomposites and carbon nanotube mechanics have also been attempted (see Appendix A) prior to establishing this study which focuses on the incorporation of nanomaterials into low-density polyethylene (LDPE), a widely used thermoplastic synthetic polymer.

1.1 Polymers

Polymers are large molecular chains containing repeating links of monomers, which are relatively simple molecular units. Polymer chain structures are generally either linear, branched, or crosslinked, see figure 1.1., [24]. Polymers can be categorized as thermoplastic or thermosetting. Thermoplastic polymer chains are linear or branched and have the ability to flow past each other.

Crosslinked polymer chains exhibit a considerable degree of dimensional stability and are said to be thermosetting.

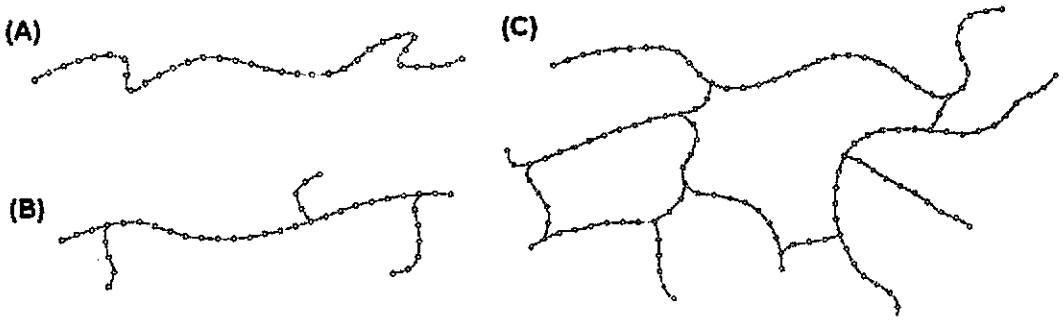

Figure 1.1: Polymer chain structures, (A) linear, (B) branched, (C) crosslinked, [24].

Polymers are found naturally in forms like DNA and proteins. However, synthetic polymers are among the most common of all materials including packaging films, textiles for clothing, rubber for tires, and the plastic articles found in everyday living [24]; as of 1990 the world consumption of synthetic materials was around 70 million metric tons, 56% being plastic material, and is slowly replacing metals for their improving physical properties, light weight, and can be processed with lower energy input [25], see figure 1.2.

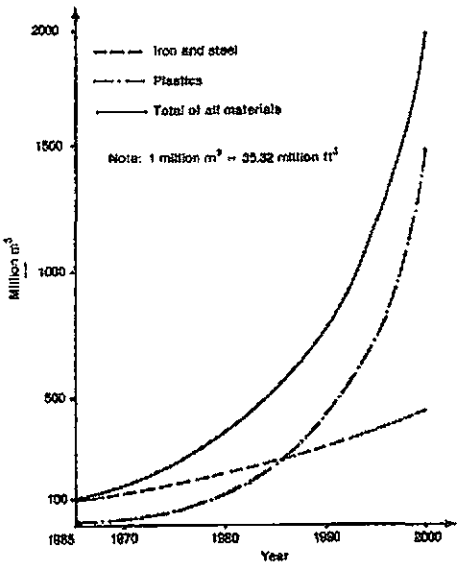

Figure 1.2: Forecast of world consumption of materials [25]

Plastics are divided into two major classifications: commodity and engineering [25]. Commodity plastics are cheap and produced in high volumes; engineering plastics are more expensive and lower in production volumes. Commodity plastics primarily consist of four major thermoplastic polymers which represent about 90% of all thermoplastics production [25].

Table 1.1: Commodity plastics [25]

Type	Abbreviation	Major uses
Low-density polyethylene	LDPE	Packaging film, wire and cable insulation, toys, flexible bottles, house wares, coatings
High-density polyethylene	HDPE	Bottles, drums, pipe, conduit, sheet, film, wire and cable insulation
Polypropylene	PP	Automobile and appliance parts, rope, cordage, webbing, carpeting, film
Poly(vinyl chloride)	PVC	Construction, rigid pipe, flooring, wire and cable insulation, film and sheet
Polystyrene	PS	Packaging (foam and film), foam insulation, appliances, house wares, toys

Low-density polyethylene is one of the widely used thermoplastic materials. It is a branched polymer consisting of repeating ethylene (CH_2) monomer units [24-25]. The LDPE used was received from Sigma-Aldrich, Inc. As table 1.2 indicates, the tensile strength, modulus, and elongation at failure for LDPE is 8.3-31 MPa, 172-283 MPa, and 100-650%, respectively.

Table 1.2: Mechanical properties of commodity plastics [25]

Polymer	Tensile Properties at Break		
	Strength (MPa)	Modulus (MPa)	Elongation (%)
Polyethylene, low-density	8.3-31	172-283	100-650
Polyethylene, high-density	22-31	1070-1090	10-1200
Polypropylene	31-41	1170-1720	100-600
Poly(vinyl chloride)	41-52	2410-4140	40-80
Polystyrene	36-52	2280-3280	1.2-2.5

Perhaps one of the most popular nanomaterial used in nanocomposites is the carbon nanotube (CNT) for its high aspect ratio, strength, stiffness, resilience, and subsequent toughness, as well as its electrical conductivity [26-32]. Composite materials containing carbon nanotubes have displayed increases in mechanical properties, as well as electrical properties. Cadmium sulfide (CdS) is a material well-known for its optical properties. Thus, CdS nanoparticles are a prime choice for making composite thin films [13].

Creating these superior composite materials, however, isn't as easy as one plus one, there are a couple of key challenges posed to researchers. Ironically,

objectives in creating nanocomposites are macroscopically the same as in concrete. In concrete, the cement is to the polymer, as the rocks are to the nanomaterial. The rocks in concrete need to be well-dispersed and bond well enough to the cement to support the load transfer. The first challenge involved homogeneously dispersing the nanomaterials avoiding any aggregation or clumping of the particles which would ultimately cause the material to weaken [8]. The three popular methods of mixing nanomaterial into polymer matrices are solution-casting, melt-compounding, and in situ polymerization [9-11]. The second challenge involved sufficiently bonding the interface of the nanomaterials to the surrounding polymer matrix [33-37]. Without this the load will not transfer to the nanomaterials and only create stress-concentrations within the material thereby weakening it. To resolve this, nanomaterials can undergo chemical functionalization; it's a process that involves attaching chemical chains to their surface which interact with the surrounding polymer matrix.

Mechanical tests are done on specimens of various geometries including dog-bone bars, thin films, and single fibers. Typical methods for fabricating polymer composites are by extrusion, casting, or some form of compression molding [25]. Extrusion and electro-spinning has been used to fabricate monofilaments in previous studies [14-16]. Characteristically, fiber materials are favored for their high strength, modulus, stretchability, thermal stability, and

spinnability among others depending on application [25]. Fibers can be applied to anything from textiles, to structural reinforcement, to cables and wires.

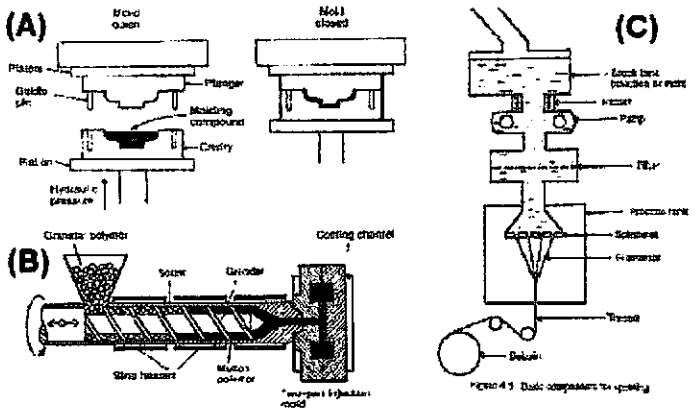

Figure 1.3: Common industrial polymer fabrication methods, (A) compression molding, (B) extrusion, (C) spinning [25].

Previous studies have shown promising results in generating nanocomposites polymer threads [14-16]. Pure carbon nanotubes threads have also been drawn out on the scale of several meters, with the yarn's toughness comparable to bulletproof vest fibers [38-41].

1.2 Nanotechnology

Nanotechnology encompasses any and all fields with at least one component on the nano-scale; one nanometer (nm), 10^{-9} m, a human hair is roughly 100,000 nm. From a mechanical standpoint, structural defects arise from the mass production of bulk materials, therein lies the heart of nanotechnology, by focusing small perfection can be obtained. Thus, atoms and molecules become the basic building blocks of fabrication [42].

A relatively new field of study, many accredit its modern conceptualization to be on December 29, 1959 at California Institute of Technology in a presentation by renowned physicist Richard Feynman entitled "There's Plenty of Room at the Bottom" [42]. In his lecture he proposed extraordinary ideas of miniaturizing computers, machines, rearranging atoms, even suggesting printing the entire Encyclopedia Britannica on the head of a pin [42]. However, the term "Nanotechnology" would not be coined until 1974 by Norio Taniguchi of Tokyo Science University [43]. Carbon nanotubes themselves were not discovered until 1991 by Sumio Iijima [42].

1.3 Motivation

This research is focused on the fabrication of high-performance nanocomposite monofilaments. The 1-dimensional structure of fibrous material, make them geometrically practical and very applicable. Fiber structures are very prevalent throughout nature. They are found in the form of spider webs and muscle tissue, and allow coconut trees to withstand hurricane force winds. Adopting nature's innovation we can make polymer-composite fibers and apply them to everything from textiles to structural reinforcements to artificial biomedical components, [25, 44]. Polymer fibers can also be engineered to retain their flexibility even under extreme sub-arctic conditions [45]. An application towards a cable modeling system [46] also inspired this research endeavor.

Cables are typically macro sized reinforcing structures. Taking that into account, it would be interesting to see its correlation to micro sized polymer composite cables. Eventually, it could even be modified and applied on the nano-level with individual CNT fibers [30-31, 47-48].

1.4 Objectives

The primary goal of this research was to successfully fabricate and mechanically test low-density polyethylene composite threads. Fabrication of the composites included the synthesis of the nanomaterials –particularly focusing on CNT, its incorporation into the polymer matrix, and the continuous yarning of the resulting composite material. Subsequently, the analysis focused on the effects of incorporating various nanomaterials at differing concentrations, and more specifically the effects of functionalizing CNT opposed to pristine CNT. The analysis focused on the material's strength, stiffness, strain to failure, and toughness properties.

CHAPTER 2

CNT SYNTHESIS

Carbon nanotubes are synthesized through three major techniques: arc discharge, laser ablations, and chemical vapor deposition [49-50]. Arc discharge produces CNT through an arc between a pair of carbon electrodes. It produces a large quantity of relatively impure CNT material, requiring further purification to isolate the CNT material. Laser ablation utilizes a laser targeting a graphite rod enclosed within an inert atmosphere. The method produces a small volume of high purity CNT, mostly single-wall carbon nanotubes (SWNT). Chemical vapor deposition (CVD) is the most common method it's relatively simple, robust, and reliable [51]. It can be scaled up for mass production of mostly multi-wall carbon nanotubes (MWNT), but can be modified to produce SWNT as well. Part of this research included the installation of a CVD system, see figure 2.1.

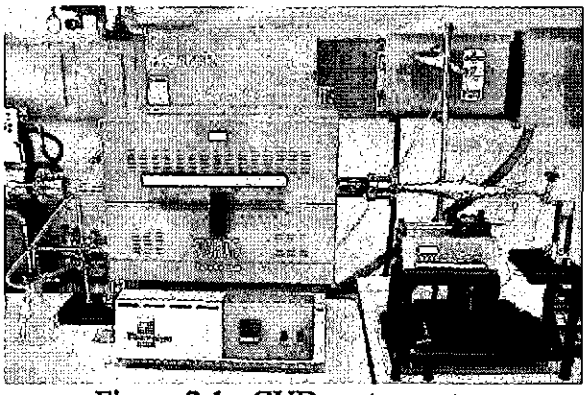

Figure 2.1: CVD system setup

The CVD method requires a vaporized carbon source injected into an inert atmosphere at a set temperature where the carbon source can decompose. The freed carbon atoms then re-structure themselves via catalyst particle onto a substrate in the form of a rolled up graphene sheet, i.e. a carbon nanotube. It is unknown as to what controls the growth mechanism of the CNT, whether the growth of the CNT from catalyst particle occurs at the root or the tip of the tube [51], see figure 2.2.

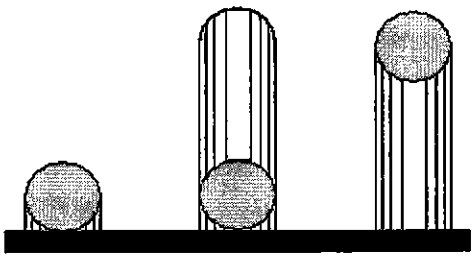

Figure 2.2: Catalyst particle growth mechanism, root growth vs. tip growth.

The CVD parameters used in this study are as follows. Argon gas flows through the system at approximately 70 to 90 cubic centimeters per minute (SCCM). The carbon and catalyst solution (100ml of xylene to 1g of ferrocene, respectively), is injected at a rate of 0.12 ml/min. into a heating cylinder set at 180 degrees Celsius. Xylene's boiling point is 140°C, subsequently, the solution is vaporized. The flowing argon gas carries the carbon/catalyst vapor into the furnace set at 770°C, where the vapor decomposes to form aligned CNTs on the substrate placed within the tube furnace. See figure 2.3.

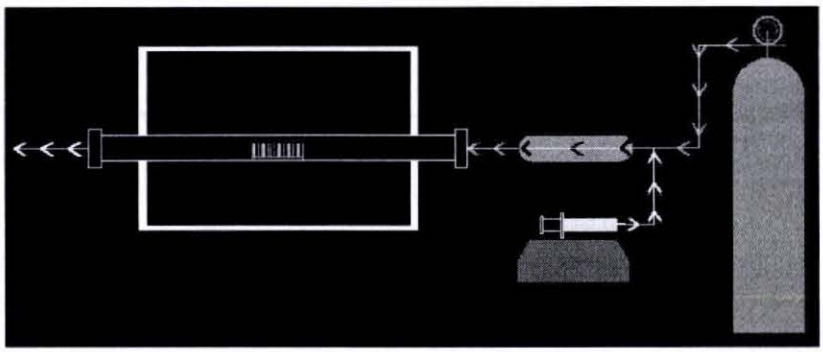

Figure 2.3: CVD system schematic, argon gas flow carries injected solution into heating cylinder for vaporization and subsequent decomposition in the tube furnace.

The furnace maybe run for as short as 15 minutes before growth is evident. In theory, CVD run times are only limited by the amount of carbon/catalyst solution and inert gas you have available at the time. There's only a 3 inch region within the furnace (approximately 5.5 in. from the furnace's intake) where CNT growth occurs, see figure 2.4. The growth rate is also not linear. While a 60 minute CVD run may yield 1mm long CNTs, a 120 minute run will not necessarily produce 2mm long CNTs. The growth rates were observed to decrease with time. The reduction maybe due to the CNT tips entangling as they get longer, and resulting in added resistance preventing growth. Figure 2.5 shows the resulting growth on a 2 cm^2 silicon dioxide (SiO_2) substrate.

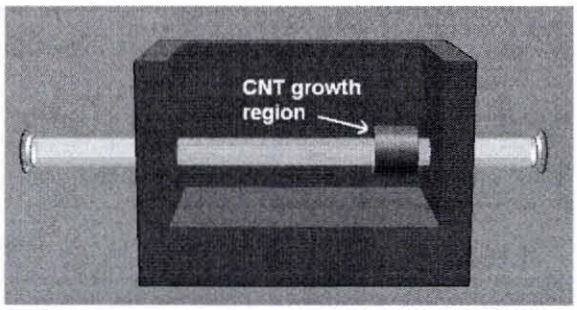

Figure 2.4: CNT growth region in CVD

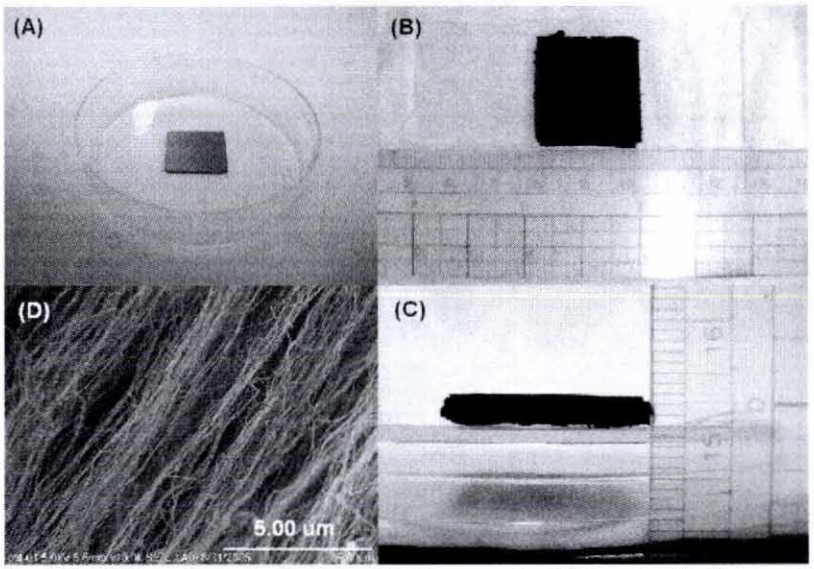

Figure 2.5: (A) SiO_2 substrate before CNT growth, (B) and (C) SiO_2 substrate after CVD, (D) SEM image of CNT growth.

There are two main types of carbon nanotubes: single-wall nanotubes (SWNT) and multi-wall nanotubes (MWNT). As the name suggests, SWNT has only one shell forming the tubular structure with a diameter between 1 and 2nm. MWNT will have multiple concentric shells forming its structure varying its diameter, as long as the diameter falls under 100nm, after which it falls in the "micro" range.

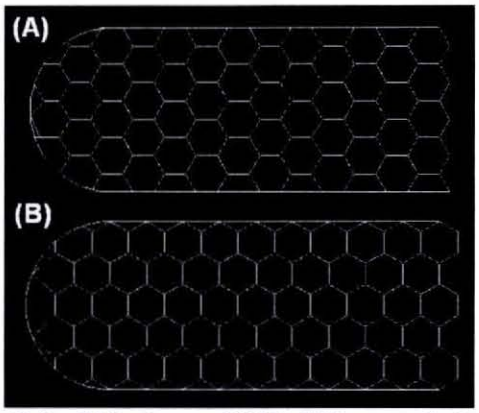

Figure 2.6: (A) zigzag CNT, (B) arm-chair CNT.

The helicity of the hexagonal carbon rings also play a roll in the general properties of CNT. If a carbon nanotube were "un-rolled", an in-plane lattice structure similar to a graphene sheet is formed. Depending on the angle of the folding procedure various properties are produced. If the sheet is rolled along the (n,0) nodes, the helicity of the nanotube is considered a zigzag formation, likewise, along the (n,n) nodes, an armchair formation is created, figure 2.6 shows the profiles of each. Zigzag CNTs have semi-conducting properties, while armchair CNTs have metallic properties. A general guideline for the relationship is shown in figure 2.7.

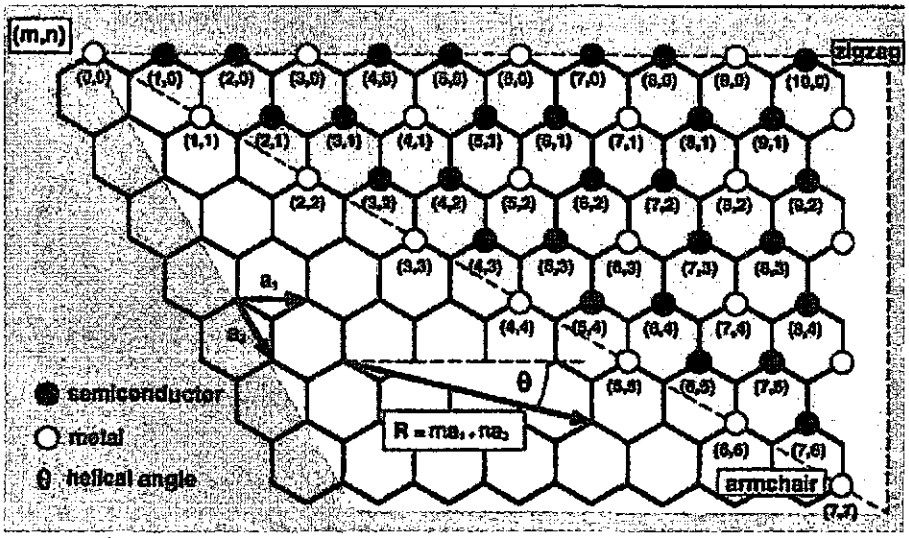

Figure 2.7: Indexing scheme showing the folding procedure for creating nanotube cylinders from planar graphene sheets [27]

CHAPTER 3

MATERIALS AND METHODS

Various nanomaterials at varying concentrations were incorporated into LDPE. A total of 7 LDPE samples were tested, shown in table 3.1. The first one was the as received LDPE from Sigma-Aldrich, Inc., referred to as the control sample (C). The next one tested was the control-xylene sample (CX). This sample underwent the same processing procedures as the following composite materials, except it excluded the nanomaterial. Functionalized single-walled carbon nanotubes (f-SWNT) were incorporated into LDPE at only one concentration, 0.05% by weight. As received, pristine, single-walled carbon nanotubes (SWNT) were incorporated into LDPE at two concentrations 0.05% and 0.5% by weight. Cadmium sulfide nanoparticles (CdS) were also incorporated into LDPE at the concentrations, 0.05% and 0.5% by weight (wt.). Attempts were made to incorporate the multi-wall carbon nanotubes as produced from the CVD setup. However, those attempts were unsuccessful. The following will go over the processing of the nanomaterials used, incorporating them into the polymer matrix, the fabrication of LDPE monofilaments, and subsequent testing of the fibers using ASTM D3822 [52] as a guideline.

Table 3.1: List of tested LDPE samples

Tested Samples	Abbreviation	Description
Control	C	As received LDPE
Control-xylene	CX	Processed LDPE without nanomaterials
Functionalized SWNT	f-SWNT	Processed LDPE with functionalized SWNT, concentrations at 0.05% wt.
Pristine SWNT	SWNT	Processed LDPE with as-received SWNT, concentrations at 0.05% and 0.5% wt.
Cadmium sulfide nanoparticles	CdS	Processed LDPE with cadmium sulfide nanoparticles, concentrations at 0.05% and 0.5% wt.

3.1 Nanomaterials

Single-walled carbon nanotubes and cadmium sulfide nanoparticles were the two types of nanomaterials tested. Two variations of SWNT were investigated, the SWNT as received from the manufacturer (Carbon Nanotechnology Inc., USA) and functionalized SWNT (f-SWNT). The f-SWNT were chemically modified in the lab. Two concentrations of SWNT and CdS particles in LDPE were prepared, 0.05% and 0.5% by weight, and one concentration of 0.05%wt. of f-SWNT in LDPE was prepared. The functionalization of SWNT, synthesis of CdS nanoparticles, and incorporation of SWNT/CdS into polymers are described in the following.

3.1.2 Functionalization of SWNT:

One of the goals of this study was to homogeneously disperse SWNT and effectively graft them to the polymer matrix. This could be done by functionalizing

the SWNT surface with additional polymer chains. Functionalization is a general term referring to any modifications done to the surface structure of CNT. The process is two-stage; first an acid-treatment, then treatment with octadecylamine (ODA). Acid treatment was involved to "cut" the SWNT and remove amorphous carbon, as well as, catalyst residue, and attach carboxyl acid groups (-COOH) to SWNT surface making it soluble in water and other high polarity solutions [33], see figure 3.1. The second treatment adds a long amine chain to the carboxyl acid branches, see figure 3.1. ODA functionalization renders the SWNT a good solubility to organic solvents [34], such as acetone, benzene, and xylene. This is useful for later incorporating nanomaterials into LDPE by processing in xylene.

To perform the acid treatment of SWNT, a ratio of 1 part nitric acid to 3 parts sulfuric acid was mixed. After including the pre-determined weight of SWNT, the acidic solution was sonicated for approximately 10 hours. To extract the SWNT from the solution, a water vacuum filtration of the acidic solution was passed through 0.5 um pore size PTFE membrane filter paper. Prior to filtration the acidic solution was diluted to avoid excessively damaging the filter paper. It took a few hours to filter all the SWNT solution. Once completed, the SWNT on the membrane were washed by passing water repeatedly through the membrane until a neutral pH value was obtained. The acid treated SWNT were then removed from the membrane.

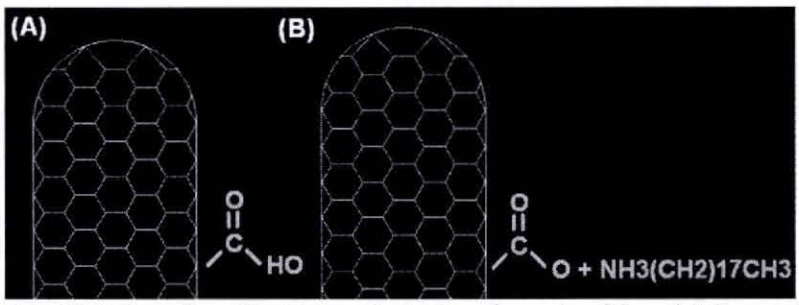

Figure 3.1: CNT functionalization: via (A) carboxyl acid and (B) octadecylamine

In the second step, the acid-treated SWNT were put into a small glass beaker and covered with ODA powder, and the powder was spread to completely cover the SWNT. The beaker was heated to 120°C to melt ODA melted and mix with the SWNT thoroughly. After the reaction, the excess ODA was removed by sonication in ethanol, a good solvent for ODA. The ethanol-ODA-SWNT solution was filtered via water-vacuum through a 0.5um pore size PTFE membrane filter to obtain functionalized SWNT. The volume of SWNT has expanded significantly due to intercalation of ODA between tubes/bundles. The functionalized samples were dried in a hood at room temperature over night.

3.1.2 CdS Synthesis:

The CdS nanoparticles used in this study were synthesized by solution processing in the lab. The incorporation of CdS into LDPE did not require additional functionalization because the as-synthesized CdS particles have amine chains wrapped around them, that is useful for dispersion in LDPE. The following will briefly go over the synthesis procedure.

First, 1 mmol of cadmium chloride ($CdCl_2$) was dissolved in 10ml of oleylamine. The $CdCl_2$ solution was heated for 30min at 180°C under an inert argon atmosphere. Then a 5ml oleylamine solution with 6mmol of dissolved sulfur was poured into the $CdCl_2$ solution. The solution was allowed to react while stirring at 180oC for 3hrs. After that, the reaction was quenched by pouring the solution into a large volume of toluene at room temperature. Finally, the CdS nanoparticles were separated from the toluene through the addition of ethanol and subsequent centrifugation. Figure 3.2 shows a transmission electron microscope (TEM) image of CdS nanoparticles with uniform diameter of 7-8 nm. The aforementioned stabilization wrapped the oleylamine chains around the CdS nanoparticles eliminating the need for any functionalization.

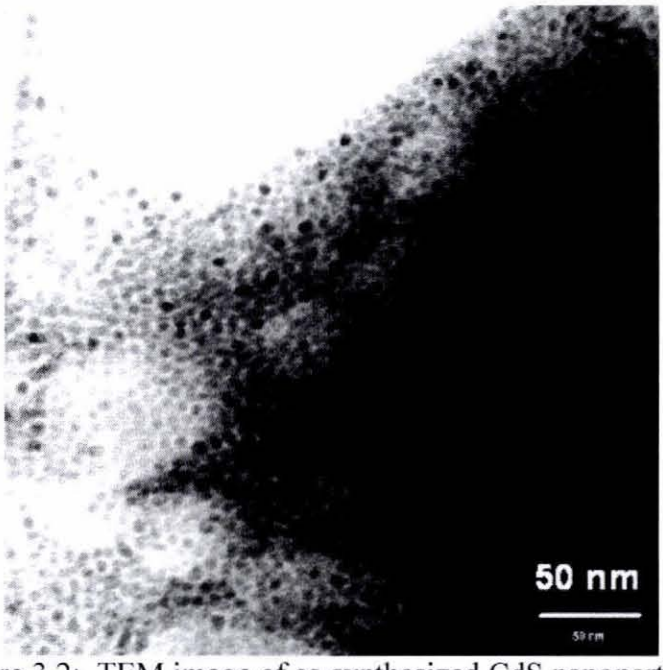

Figure 3.2: TEM image of as-synthesized CdS nanoparticles

3.2 Incorporation of Nanomaterials into Polymers

A pre-determined weight of nanomaterial (f-SWNT, SWNT, or CdS) was mixed with approximately 10ml -15ml of xylene. The solution was sonicated for about 30 minutes. The well-dispersed solution and 5g of LDPE pellets were added into a Florence flask partially submerged in a silicon oil bath on a hotplate. Figure 3.3 shows the instrument setup.

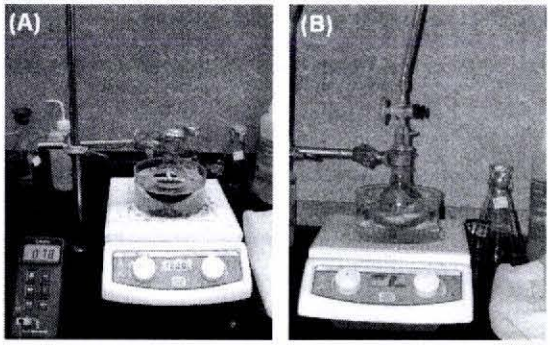

Figure 3.3: (A) Dilution of LDPE with xylene and low heat, (B) Xylene extraction through vacuum pump and heat

The hotplate temperature was set at approximately 80-90°C with a magnetic stir bar mixing the solution for about 60 minutes. The combination of heat and xylene will melt the LDPE pellets. After that, the magnetic stir bar was removed and the solution left to cool overnight while excess xylene evaporated under a chemical fume hood. The solution partially solidifies, the remaining xylene solvent weakens the polymer bonds and prevents it from completely hardening. But now the CNTs are homogeneously blended within polymer matrix. The next step will remove the remaining xylene from the material.

To remove the remaining xylene from the polymer, we used a vacuum pump and additional heat from the hotplate. The flask with polymer composite sample was partially submerged in an oil bath heated to about 120 to 140°C. With a vacuum distillation adapter covering the flask, the vacuum hose of an Alcatel 2005 SD vacuum pump was attached. As the polymer composite melts, the remaining xylene is evaporated and sucked out of the system through the pump, see figure 3.3. The hotplate remained at 120 to 140°C for at least 2.5 hours, until a visual confirmation can be made that no further liquid is being evaporated and all air-bubbles have been brought to the surface of the viscous polymer composite fluid. The hotplate was turned off and the sample cooled and solidified.

Finally, the sample was removed from the flask by cutting away chunks with a scalpel. Figure 3.4 shows the LDPE before and after nanomaterial incorporation. After removing the sample, the chunks of the bulk composite material was weighed to compare with original weight. This would confirm the removal of the xylene. A slight decrease in the original weight was expected due to residual losses.

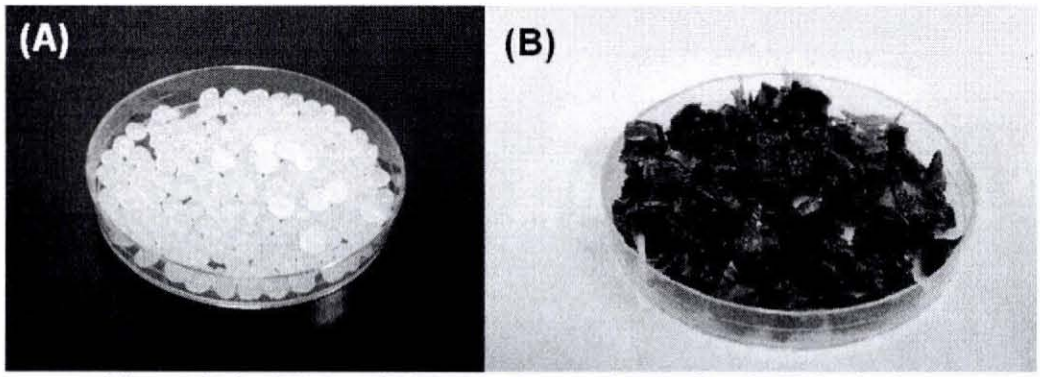

Figure 3.4: (A) 5g of LDPE before and (B) after CNT inclusion

3.3 Continuous Yarning of Nanocomposites

Fine single filaments of composite polymers were drawn out by pultrusion. Technically, pultrusion is a composite manufacturing method where a fiber reinforced material is pulled through a resin impregnation bath and cures in a shaping die. It's a fabrication method similar to extrusion except in this case the polymer is not being pushed, and no die is used to form the profile of the polymer melt. As a result, there was no precise control over the cross-section of the drawn out polymer composites.

Once the bulk composite was obtained they were placed in a glass beaker and melted down once more over a hotplate at 110 °C. Figure 3.5 shows the melting of f-SWNT-0.05%. A spool was placed above the beaker. With a pair of tweezers, a small amount of melted polymer was pulled over the spool. The spool rotated to wind up continuous fine filaments of LDPE composites. Figure 3.6 shows the equipment setup.

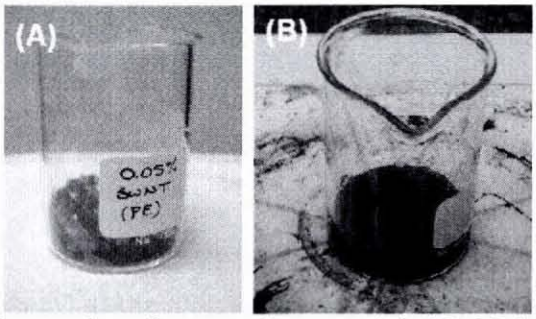

Figure 3.5: (A) Solid granules of composite material, (B) Melting the bulk composite material

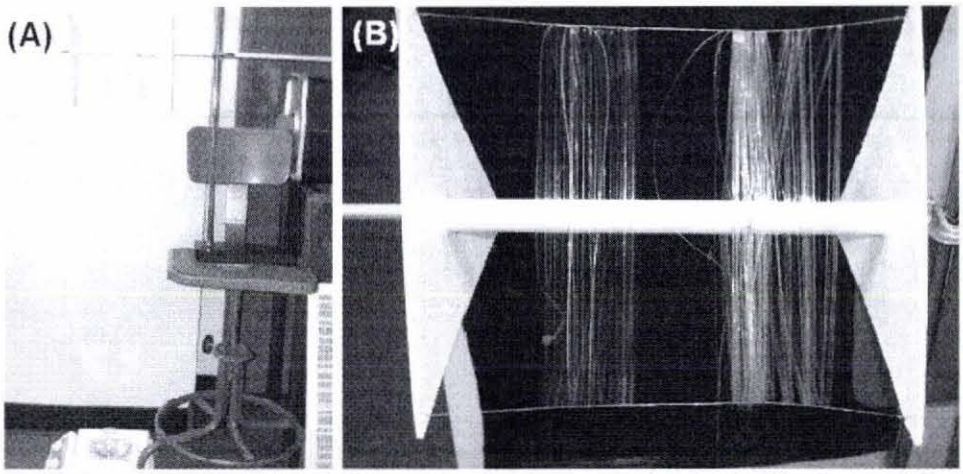

Figure 3.6: (A) Instrument setup to spool the composite monofilaments, (B) close up of wound monofilaments.

A key issue to the process was controlling the cross-section because there is no shaping die to form the cross-section's profile. A couple of aspects directly affecting this are the spool's rotation speed and the initial pinch of the polymer to start winding. The spool's rotation was done by hand, the faster the spool rotated the skinnier the thread, likewise slower rotation yielded thicker threads. Naturally, the skinnier the thread the closer their cross-section comes to circular. But the process was able to produce many meters of continuous nanocomposite yarns. Figure 3.7 shows all of the tested monofilaments and individual strands of each; the samples are from left to right: control, control-xylene, f-SWNT-0.05%, SWNT-0.05%, SWNT-0.5%, CdS-0.05%, and CdS-0.5%.

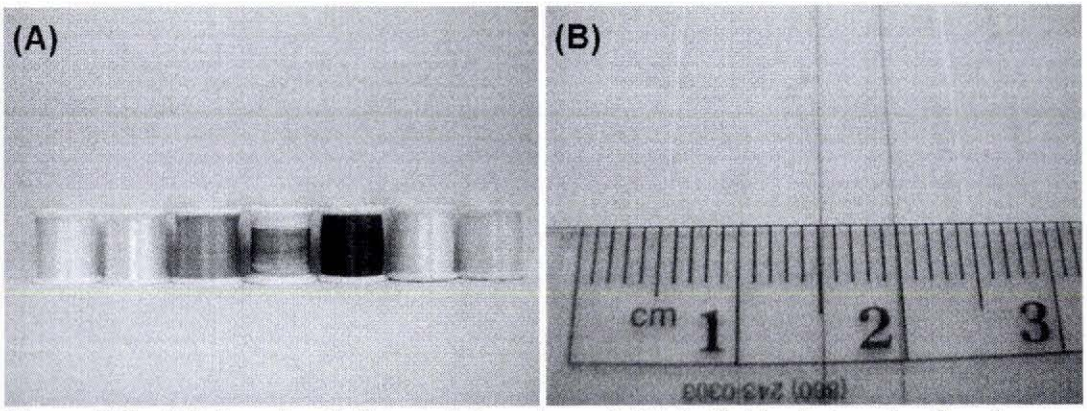

Figure 3.7: (A) Spools of all tested threads, and (B) individual strands of each tested thread, from left to right: control, control-xylene, f-SWNT-0.05%, SWNT-0.05%, SWNT-0.5%, CdS-0.05%, CdS-0.5%

3.4 Mechanical Testing

Mechanical testing yielded data such as stress-strain curves. A material's behavior under loading can be identified on the curve. Figure 3.8 shows the general shape of the stress-strain curve of a tensile test symbolic of mild-steel, one of the most widely used structural material. This study will investigate four material properties measured from the stress-strain curve: stiffness, strength, strain to failure, and toughness.

In Figure, the slope of OA determines the stiffness of the material or modulus of elasticity, commonly known as Young's modulus. Point A is the proportional limit. If the load is removed within this region, the material remains elastic and will return to its original shape.

Beyond the proportional limit, yielding will occur at point B to C. From C to D, the atomic structure of the material starts to realign to resist further deformation. This region is called strain hardening. At point D, the second point of

interest, the material reaches its ultimate tensile stress, also referred to as ultimate strength. From point D to E, the material begins to neck as the cross-section becomes visibly thinner before the failure at point E. The third quantity of interest is at point F, the strain at failure, called the strain to failure value.

The fourth quantity is toughness, also called strain-energy. It is the amount of energy a material can absorb before rupturing, and can be calculated by the integral of the stress-strain curve. It's given in units of energy per volume.

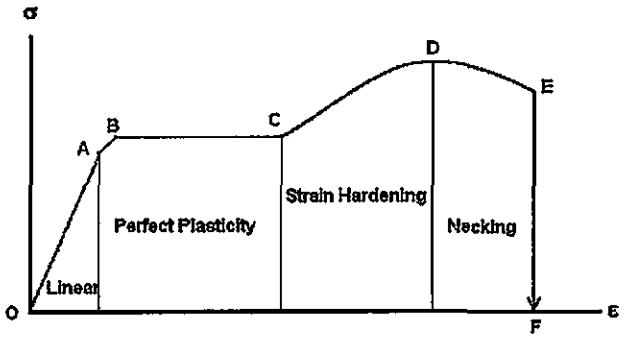

Figure 3.8: Typical stress-strain curve [53].

3.4.1 Testing Guidelines

The American Society for Testing and Materials standard test method for tensile properties of single textile fibers, ASTM D3822, provided the guidelines for the following test [52]. Parameters such as the type of tensile test, the rate of extension, load cell capacity, connection type, and specimen mounting were all given in the standard.

ASTM D3822 uses a constant rate of extension (CRE) tensile testing machine, the rate is determined by the gage length. Rate of extensions are given as

10%, 60%, and 240% of the initial gage length per min, if the specimen is expected to strain 8%, 8 to 100%, or over 100% respectively. The test requires a minimum gage length of 10mm, but other popular lengths include 20, 25, and 250mm.

ASTM D3822 states to ensure an accurate recording of the test data, specimen's failure load needs to fall between 20 and 90% of the machine's capacity, although 50-90% is preferred. This capacity is controlled by an interchangeable load cell. Another key parameter is the connections holding the specimen in place during the test. The grips holding the specimen should be flat jaws designed to minimize the slippage of single fibers.

ASTM D3822 dictates if the specific grips aren't available, the tips of the specimen maybe may be cemented to tabs to be held by the available grips. The tabs and cementing technique should not interfere with the integrity of the data plot nor the specimen itself. Therefore the tab should be of a thin plastic, cardboard, or similar material that won't elongate relative to the tested fiber, and the cementing should be bonded well enough to prevent slippage during the test.

3.4.2 Testing Procedure

The CRE tests were performed using an Instron 4206 materials testing machine with a 500N static load cell. The estimated failure of the specimens were about 1N, therefore, a 5N load cell would've been ideal. The available specimen

grips for the 500N load cell were not designed to hold fibers, rather they were used for holding flat bars, and dog-bone specimens, see figure 3.9.

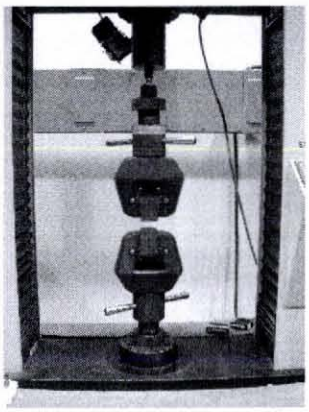

Figure 3.9: Instron 4206 tensile testing machine setup

Tabs were cut from a poster board to secure each specimen. The 1-1/4" x 1-1/2" (31.75mm x 38.1mm) tabs had a centrally located die cut circle measuring 16mm in diameter. Each specimen was attached using a hot glue stick along the middle of the tab's length. Bonding the LDPE specimens proved particularly difficult as epoxy and most adhesives do not bond well to the smooth surface of polyethylene. A hot glue gun ended up being the best bonding tool for polyethylene, as it melts the material onto the tab, securing it with minimal slippage, see figure 3.10.

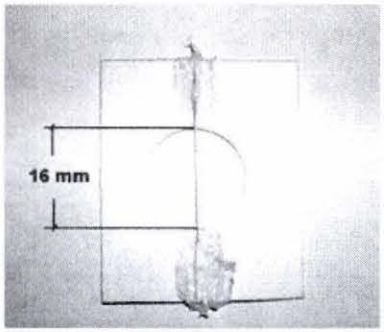

Figure 3.10: Typical specimen mounted on cardboard tab boded with hot glue.

With the single fiber spanning the full diameter of the circle, the span across the circle now becomes the specimen's gage length. Assuming LDPE will elongate more than 100% of its initial length; the rate of extension is set to be 240% of the initial length per minute, or 38.4 mm/min. After clamping the tab in place, the outer edges of the tab are cut across to the inner edge of the circle prior to testing, see figure 3.11.

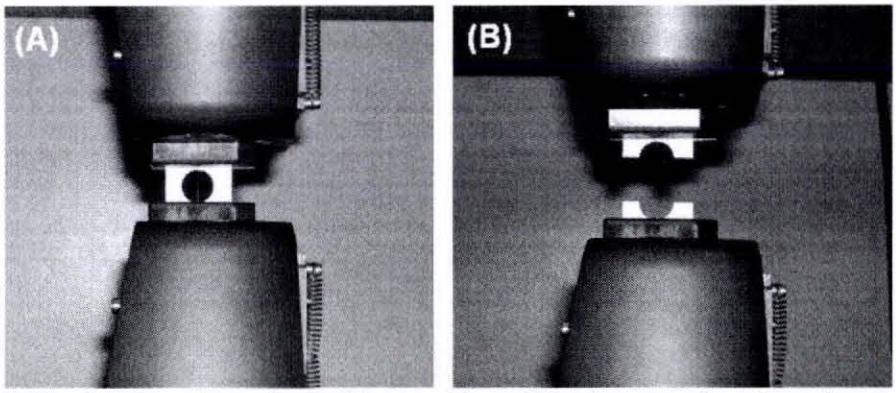

Figure 3.11: (A) Specimen loaded in machine, (B) tab cut and undergoing test.

Data was collected for 5 specimens of each LDPE sample type. Data acquisition was a three-step process. First, a load-extension curve was directly plotted given the position of the machines crosshead as it performs the tensile test, and the load experienced by the load cell. Then, the fractured pieces were mounted and prepared for scanning electron microscopy (SEM) imaging. The SEM images were interpreted to obtain the cross-sectional areas of each specimen used to plot the stress values from the load-extension data. The strain values are calculated based on the set gage length of the tabs and the extension of the machine's crosshead. Ideally, an extensometer is used to accurately obtain the strain values.

However, given the size of the specimens, there wasn't an extensometer readily available for use in the lab to perform on such a scale. As a result, the strain values are based on the movement of the machine's crosshead, and errors can occur due to slippage at the specimen grips. Finally, based on the preceding methods, a stress-strain curve was plotted using the load-extension data set.

CHAPTER 4

RESULTS

Data was obtained for 5 specimens per tested sample. SEM analysis was done to get the cross-section values for each specimen. The measured width of the monofilaments from the SEM images was used to calculate the cross-sectional values to plot the stress-strain curve of each test. Based on the stress-strain curves the material properties of strength, stiffness, strain to failure and toughness were determined.

4.1 SEM Characterization

The fractured plane of the tested fibers were viewed under a Hitachi S-800 scanning electron microscope (SEM), figure 4.1 shows a typical image of each of the tested samples (see Appendix B for complete collection of SEM images). Higher magnifications of the fractured surfaces revealed fiber-like strands which could possibly be bundles of polymer chains. All specimens were cut from a continuous span of their respected composite sample, except for two of the control-xylene specimens that were cut from a thicker section. This was done to demonstrate the correlation between the load-extension curve (see Appendix C) recorded during the test and the stress-strain curves plotted after obtaining the cross-section values.

Measuring the cross-sectional area of the specimens proved particularly challenging because there was no control over the cross-section during the monofilament fabrication process. Because specimen profiles could vary from specimen to specimen, as well as vary throughout any given length, it was important to apply the cross-sectional profile of the tested specimen to specifically that specimen.

Methods to measure the area, via SEM, prior to tensile tests would compromise the integrity of the specimen. In order to accurately account the cross-section, the specimen needs to be snapped under cryogenic conditions. This ensures a clean break to see the true cross-section, opposed to simply cutting it which will show a smashed, crimped cross-section. Then the specimen needs to be prepared with a thin layer of gold in order to be seen under the SEM. All these procedures make it impossible to measure the cross-section prior to testing via SEM without compromising the specimen's integrity.

The next viable option was to measure it after testing. Initially it was thought the material properties could be obtained from a true stress-strain curve based on the fractured surface area of the specimen. However, this cross-sectional area is only the area at failure, and does not account for the progressively decreasing cross-sectional area the specimen experiences throughout the test. Therefore, if only the final cross-section at failure is applied across the entire test, the initial stresses will be much larger.

The method settled upon used the perceived width near the fractured surface as the diameter of the tested monofilament. This assumes an initially circular cross-section; however, some specimens were more circular while some were more elliptical, depending on the perspective which the SEM image was taken. This would greatly affect the interpretation of the overall cross-sectional area and consequently all material properties based on this measurement. In addition, using this post-test measuring method doesn't account for the possibility of necking of the specimen. Nevertheless, this method was determined to be the best option based on the means available at the time.

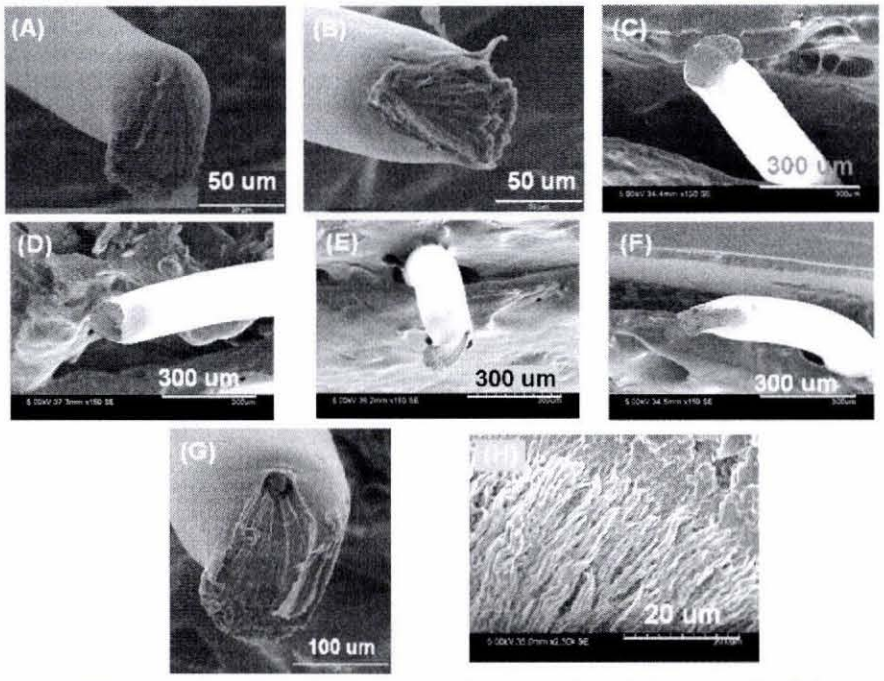

Figure 4.1: SEM images of typical composite samples, (A) control, (B) control-xylene, (C) f-SWNT-0.05%, (D) SWNT-0.05%, (E) SWNT-0.5%, (F) CdS-0.05%, (G) CdS-0.5%, (F) close up of fracture plane.

Table 4.1: Circumferential area of each specimen.

Sample	Circ.Area (mm^2)
Control-3b	0.00315
Control-4b	0.00359
Control-2ba	0.00348
Control-5ba	0.00456
Control-5bb	0.00471
Std. Dev.	0.00069

Sample	Circ.Area (mm^2)
Control-X-2	0.03323
Control-X-4	0.02446
Control-X-5	0.01968
Control-X-6	0.00629
Control-X-8	0.01042
Std. Dev.	0.01082

Sample	Circ.Area (mm^2)
f-SWNT-0.05%-3a	0.04544
f-SWNT-0.05%-4a	0.01674
f-SWNT-0.05%-1a	0.01191
f-SWNT-0.05%-2ab	0.01757
f-SWNT-0.05%-5ab	0.02628
Std. Dev.	0.01327

Sample	Circ.Area (mm^2)
SWNT-0.05%-2	0.02241
SWNT-0.05%-5a	0.03122
SWNT-0.05%-1a	0.01926
SWNT-0.05%-2a	0.02533
SWNT-0.05%-4a	0.01827
Std. Dev.	0.00523

Sample	Circ.Area (mm^2)
SWNT-0.5%-1	0.01792
SWNT-0.5%-1a	0.01101
SWNT-0.5%-2a	0.00958
SWNT-0.5%-4a	0.01066
SWNT-0.5%-5a	0.01098
Std. Dev.	0.00334

Sample	Circ.Area (mm^2)
CdS-0.05%-4a	0.01844
CdS-0.05%-1a	0.01608
CdS-0.05%-5a	0.01537
CdS-0.05%-3ab	0.01428
CdS-0.05%-2ad	0.01953
Std. Dev.	0.00218

Sample	Circ.Area (mm^2)
CdS-0.5%-1	0.06325
CdS-0.5%-3a	0.03328
CdS-0.5%-1a	0.03600
CdS-0.5%-4ab	0.02785
CdS-0.5%-5ab	0.02573
Std. Dev.	0.01512

A Hummer 6.2 sputter coater was used to coat the LDPE specimens with a thin layer of gold for SEM observation. The sputtered gold is estimated to be only a few nanometers thick, it is negligible in calculating the cross-section of the specimens.

The SEM images like figure 4.10 reveal certain key points the monofilaments undergo as they stretch and fail. As the fiber stretches the lateral contraction is evident especially near the region of failure. Images in figure 4.10 also show radial patterns at the fractured surface, this is believed to be the effect of shearing on the fiber during the test.

4.2 Tensile Stress-Strain Curves of Nanocomposite Monofilaments

The stress-strain curves were obtained using the Bluehill 2 software integrated with an Instron 4206 materials testing machine. The load cell was originally designed for use 100 times out of range of the micro sized LDPE filaments; as a result, there was a lot of noise produced in the curves. The following figures show the tested specimens of each composite sample; subsequent curves per sample are offset for display purposes. All specimens failed within the span between the grips and not at the grips (where stress concentrations might occur).

Table 4.2: Mechanical properties of control specimens

CONTROL				
Sample	Tensile Strength (MPa)	Tensile Strain	Modulus (MPa)	Toughness (MJ/m^3)
3b	167.14891	3.80737	406.11176	543.11
4b	120.9851	2.30743	198.63882	255.242
2ba	105.90055	2.21942	247.69832	203.998
5ba	103.91608	2.16751	124.7358	196.727
5bb	86.63582	1.61133	146.65762	89.304
Average	**116.917292**	**2.422612**	**224.768464**	**257.6762**
Std. Dev.	30.60690352	0.820878206	112.0287524	170.6046097

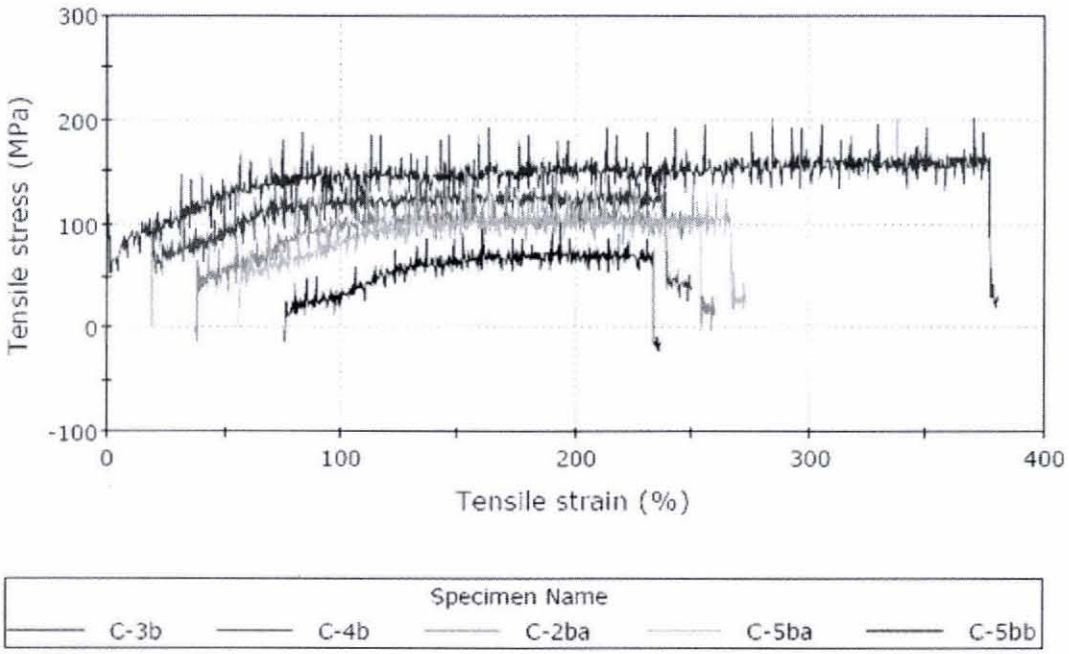

Figure 4.2: Control stress-strain curves

The tensile strength of the unprocessed control specimens is much larger than the expected published values. The tensile strength was previously stated as 8.3-31 MPa. The reason for the discrepancy is possibly due to taking cross-section measurements after the tensile tests where the cross-sections likely reduced which correlates to higher stress-values.

All specimens were taken from the same continuous span of the control sample. Note the slight variation between the stress-strain and load-extension curve (Appendix C), this is possibly due to the methodology of cross-sectional measurements. Also note the beginning offset of each subsequent curve, thus the strain-to failure values are also offset. There's a general trend for a large plastic region to occur with no significant strain-hardening before failure.

This graph was particularly noisy because the loading remained at or below 0.5N, considering this load cell's capacity is 500N, the resolution will decrease with the application of smaller loads. The load-extension data and graphs are available in Appendix C.

Table 4.3: Mechanical properties of control-xylene specimens

CONTROL-XYLENE				
Sample	Tensile Strength (MPa)	Tensile Strain	Modulus (MPa)	Toughness (MJ/m^3)
2	28.38804	0.92734	101.77562	18.488
4	32.7088	0.85933	127.39238	21.166
5	29.73166	0.65119	147.84274	13.155
6	68.34279	1.19336	195.72145	65.974
8	34.37767	0.99935	80.88676	26.683
Average	**38.709792**	**0.926114**	**130.72379**	**29.0932**
Std. Dev.	16.73349317	0.198008048	44.3017456	21.18572313

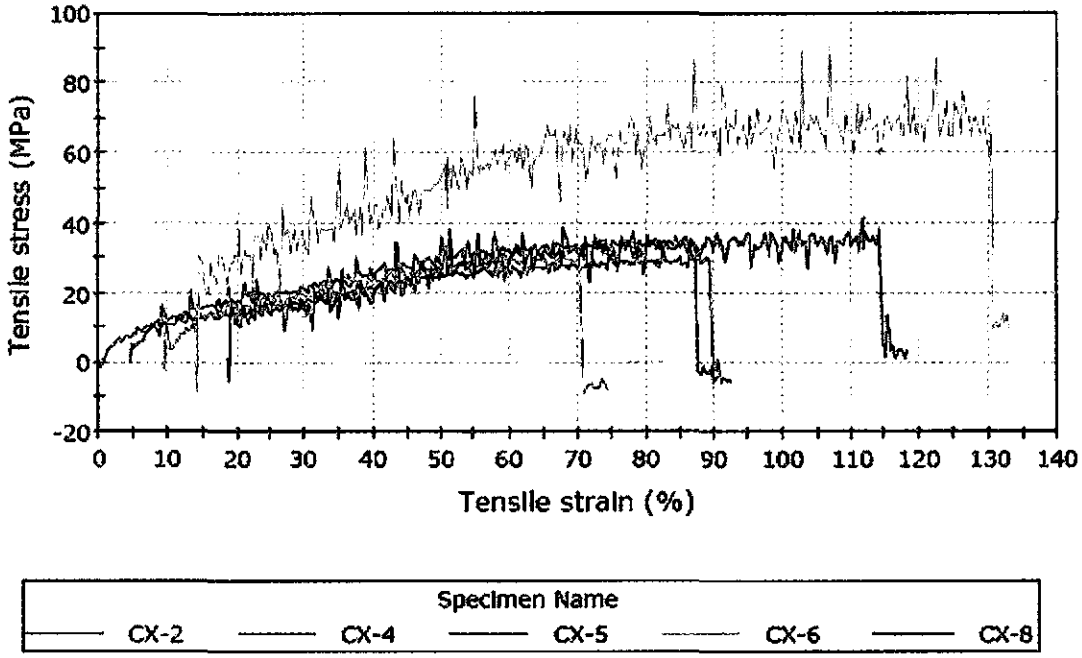

Figure 4.3: Control-xylene stress-strain curves

As previously mentioned, two CX samples were cut from a thicker section to demonstrate the correlation between the load-extension curve (see Appendix C) recorded during the test and the stress-strain curves plotted after obtaining the cross-section values. Specimen CX-2 and CX-4 were taken from thicker span of CX monofilament samples. CX-2 and CX-4 required a significantly larger load to fracture, as seen in the load-extension data and graph the effects of the cross-section measurements are noticeable in the stress-strain curve. Except for specimen CX-6, most of the specimens correlate to one another, including CX-2 and CX-4. Note the beginning offset of each subsequent curve, thus the strain-to failure values are also offset. There also seems to be a slight plastic region before failure.

Table 4.4: Mechanical properties of f-SWNT-0.05% specimens

FUNCTIONALIZED SWNT 0.05%				
Sample	Tensile Strength (MPa)	Tensile Strain	Modulus (MPa)	Toughness (MJ/m^3)
3a	21.28568	2.12739	97.56374	39.596
4a	61.34507	3.1634	296.95049	172.037
1a	63.164	3.37526	304.21626	189.479
2ab	50.97101	2.2309	230.79949	101.732
5ab	30.44358	2.93934	139.09181	80.859
Average	**45.441868**	**2.767258**	**213.724358**	**116.7406**
Std. Dev.	18.74851507	0.559758451	92.83081372	62.87408705

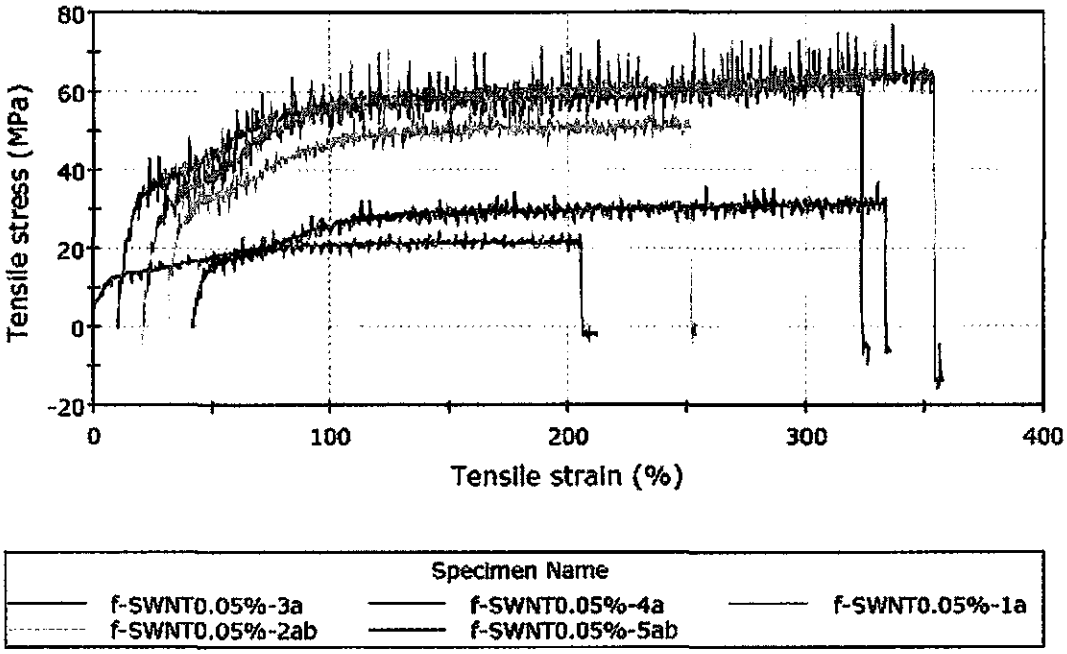

Figure 4.4: f-SWNT-0.05% stress-strain curves

All specimens were taken from the same continuous span of the f-SWNT-0.05% sample. Note the discrepancy between the stress-strain and load extension curves, see Appendix C. If all the specimens were taken from the same continuous span, both curves should mimic each other fairly well, however, that's not the case presumably due to the cross-sectional measurement methodology. The graph's resolution is slightly smoother due to the larger loads being applied. Also note the beginning offset of each subsequent curve, thus the strain-to failure values are also offset on the graph. There's a general trend for a large plastic region to occur before failure. Specimen f-SWNT-0.05%-4a appears to have some strain-hardening effect before failure; the other specimens do not exhibit significant strain-hardening before failure.

Table 4.5: Mechanical properties of SWNT-0.05% specimens

PRISTINE SWNT 0.05%				
Sample	Tensile Strength (MPa)	Tensile Strain	Modulus (MPa)	Toughness (MJ/m^3)
2	31.43728	1.31943	112.49302	28.937
5a	27.53851	1.26333	126.9772	27.058
1a	42.78007	1.0307	156.42524	32.105
2a	34.88509	1.13125	133.18431	31.322
4a	47.71308	1.06334	166.35533	37.173
Average	**36.870806**	**1.16161**	**139.08702**	**31.319**
Std. Dev.	8.261844951	0.12546938	21.98240868	3.831356353

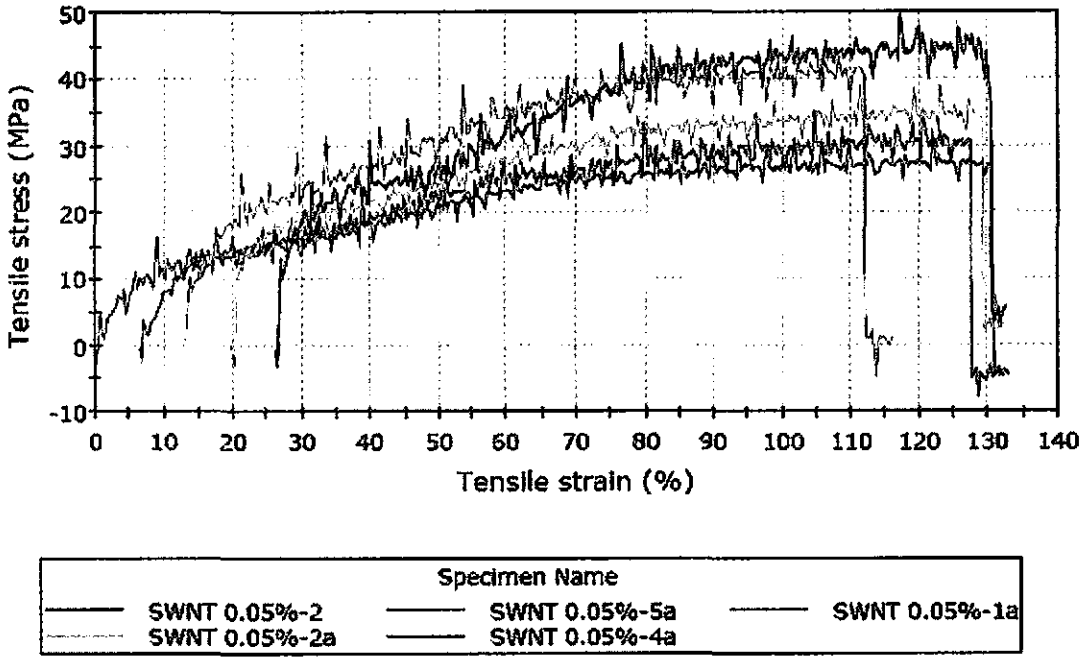

Figure 4.5: SWNT-0.05% stress-strain curves

All specimens were taken from the same continuous span of the SWNT-0.05% sample. Note the discrepancy between the stress-strain and load extension curves, see Appendix C. If all the specimens were taken from the same continuous span, both curves should mimic each other fairly well, however, that's not the case presumably due to the cross-sectional measurement methodology. The graph's resolution appears slightly smoother due to the larger loads being applied. Note the beginning offset of each subsequent curve, thus the strain-to failure values are also offset on the graph. There is relatively little plastic behavior exhibited in this sample.

Table 4.6: Mechanical properties of SWNT-0.5% specimens

PRISTINE SWNT 0.5%				
Sample	Tensile Strength (MPa)	Tensile Strain	Modulus (MPa)	Toughness (MJ/m^3)
1	25.98685	2.0835	103.05642	47.786
1a	59.649	2.56732	216.62497	111.084
2a	71.04619	2.14349	266.64986	125.908
4a	49.28513	1.55134	203.25941	64.645
5a	43.50183	2.2194	168.79887	86.298
Average	**49.8938**	**2.11301**	**191.677906**	**87.1442**
Std. Dev.	16.99527543	0.365714871	60.73404974	32.1393224

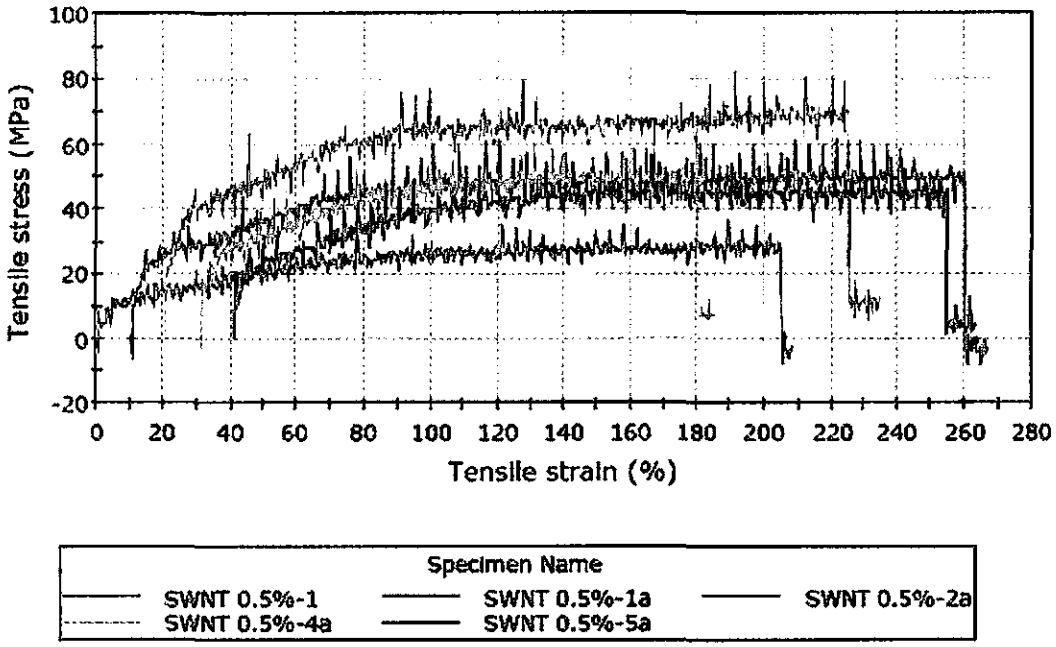

Figure 4.6: SWNT-05% stress-strain curves

All specimens were taken from the same continuous span of the SWNT-0.5% sample. Note the discrepancy between the stress-strain and load extension curves, see Appendix C. If all the specimens were taken from the same continuous span, both curves should mimic each other fairly well, however, that's not the case presumably due to the cross-sectional measurement methodology. This graph's

resolution is moderately noisy due to the 500 N load cell fluctuating around a relatively low 0.7 N. Also note the beginning offset of each subsequent curve, thus the strain-to failure values are also offset on the graph. There's a general trend for a large plastic region to occur with no significant strain-hardening before failure.

Table 4.7: Mechanical properties of CdS-0.05% specimens

CdS 0.05%				
Sample	Tensile Strength (MPa)	Tensile Strain	Modulus (MPa)	Toughness (MJ/m^3)
4a	40.79627	2.23525	151.90079	82.516
1a	43.81277	1.62325	135.03402	58.371
5a	43.50691	1.42751	143.18406	52.393
3ab	58.53399	1.49076	209.44182	70.386
2ad	32.4062	2.05059	151.52384	61.803
Average	**43.811228**	**1.765472**	**158.216906**	**65.0938**
Std. Dev.	9.434205957	0.357734447	29.46232734	11.71405309

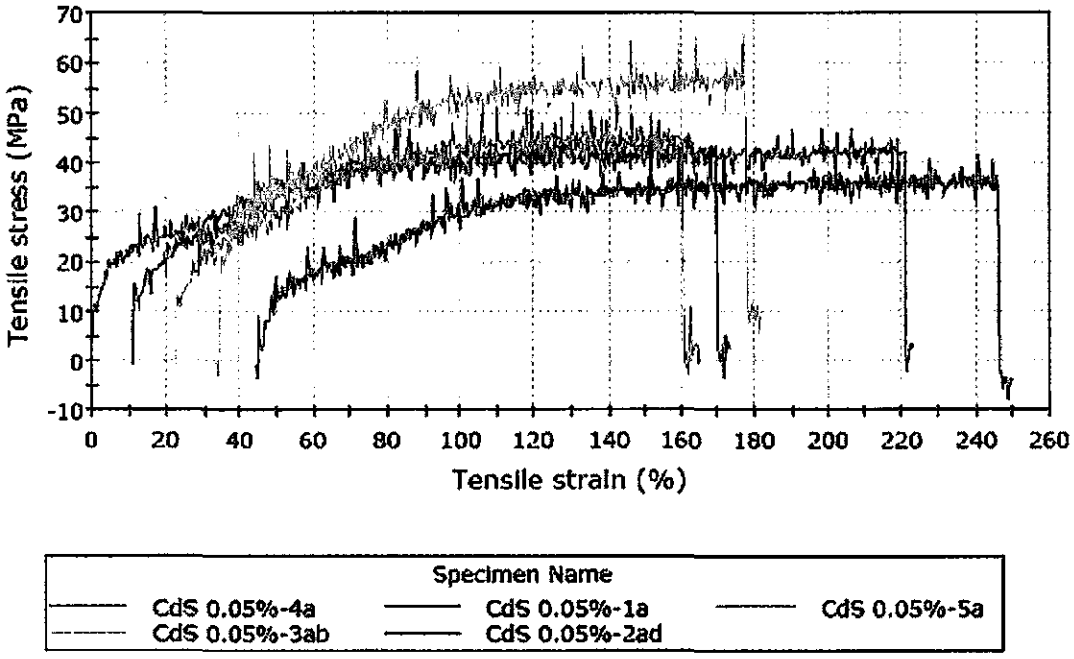

Figure 4.7: 0.05% Cadmium sulfide stress-strain curves

All specimens were taken from the same continuous span of the CdS-0.05% sample. Note the discrepancy between the stress-strain and load extension curves, see Appendix C. If all the specimens were taken from the same continuous span, both curves should mimic each other fairly well, however, that's not the case presumably due to the cross-sectional measurement methodology. This graph's resolution is slightly smoother due to the larger loads being applied. Also note the beginning offset of each subsequent curve, thus the strain-to failure values are also offset on the graph. There's a general trend for a large plastic region to occur with no significant strain-hardening before failure.

Table 4.8: Mechanical properties of CdS-0.5% specimens

CdS 0.5%				
Sample	Tensile Strength (MPa)	Tensile Strain	Modulus (MPa)	Toughness (MJ/m^3)
1	22.46616	2.62731	132.69294	52.809
3a	41.26368	2.86733	199.69175	104.789
1a	38.14598	3.16749	188.40946	107.438
4ab	39.01817	2.20335	181.13344	75.539
5ab	44.5531	2.49141	198.47377	94.884
Average	**37.089418**	**2.671378**	**180.080272**	**87.0918**
Std. Dev.	8.541181041	0.366710029	27.56344775	22.89462102

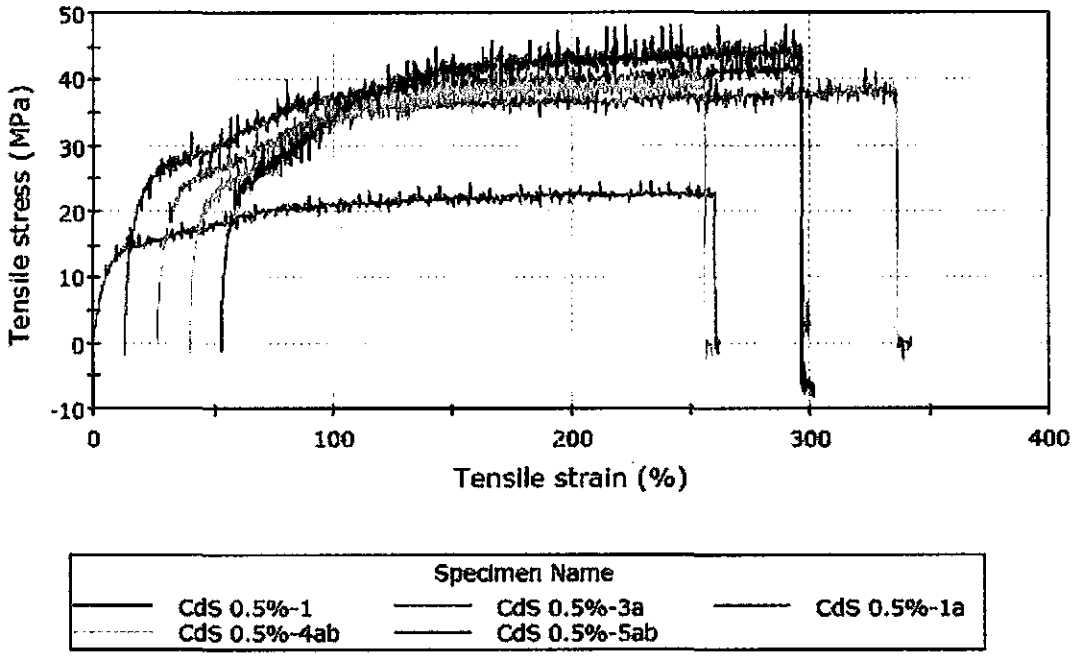

Figure 4.8: 0.5% Cadmium sulfide stress-strain curves

All specimens were taken from the same continuous span of the CdS-0.5% sample. Note the discrepancy between the stress-strain and load extension curves, see Appendix C. If all the specimens were taken from the same continuous span, both curves should mimic each other fairly well, however, that's not the case presumably due to the cross-sectional measurement methodology. This graph's resolution is slightly smoother due to the larger loads being applied. Also note the beginning offset of each subsequent curve, thus the strain-to failure values are also offset on the graph. There's a general trend for a large plastic region to occur. Specimens CdS-0.5%-3a and 1a appear to exhibit a slight strain-hardening effect before failing.

Based on the stress-strain curves, various material properties were obtained. Tensile strength, stiffness, strain to failure, and toughness of each composite sample were averaged out and compared to one another. Toughness represented by the area under the stress-strain curves were calculated using the Origin software. The remaining material property values were given by the Bluehill 2 software.

4.3 Strength, Stiffness, Strain to Failure, and Toughness

The processing of pristine LDPE in xylene degraded the material overall, comparing the two control samples. The dissolving of LDPE granules with xylene reduced the material's tensile strength, strain to failure, modulus of elasticity, and toughness by, 67%, 62%, 42%, and 89% respectively. However, it is reasonable to reference the control to be the LDPE subjected to the same processing method as its nanocomposite counterparts to reveal the effect of nanomaterials, there is an improvement in most of the measured material properties with the addition of various nanomaterials.

Tensile strength of the nanocomposite samples all decreased as compared to the pristine control sample, as seen in table 4.9. The strength of the pristine SWNT samples at 0.05%wt. and 0.5%wt. both decreased by 68% and 57% respectively; the f-SWNT sample decreased by 61%. The 0.05%wt. and 0.5%wt. CdS samples also experienced a decrease in tensile strength by 63% and 68%, respectively, compared to the control sample. However, if the nanocomposite samples were compared to

the processed control-xylene sample, table 4.10 and figure 4.9 show some improvements in the tensile strength of the materials. The SWNT samples degraded slightly then increased with the addition of more SWNT material. The addition of 0.05%wt. SWNT decreased strength by 4.75% and increased strength by 29% at 0.5%wt. SWNT. The addition of functionalized SWNT at 0.05% wt. further increased strength by 17%. Using f-SWNT at the same concentration as the pristine SWNT had an improvement of 23%. The CdS samples as compared to the processed control-xylene sample show an increase in strength of 13%, but a decrease of 4.0% at 0.05%wt. and 0.5%wt., respectively. There was a slight decline in tensile strength with an increased CdS concentration.

Table 4.9: Comparison of tensile strength relative to control

Sample	Tensile Strength (MPa)	Standard Deviation	% Difference
Control	116.92	30.61	0.00
Control-Xylene	38.71	16.73	-66.89
f-SWNT-0.05%	45.44	18.75	-61.13
SWNT-0.05%	36.87	8.26	-68.46
SWNT-0.5%	49.89	17.00	-57.33
CdS-0.05%	43.81	9.43	-62.53
CdS-0.5%	37.09	8.54	-68.28

Table 4.10: Comparison of tensile strength relative to control-xylene

Sample	Tensile Strength (MPa)	Standard Deviation	% Difference
Control	116.92	30.61	202.04
Control-Xylene	38.71	16.73	0.00
f-SWNT-0.05%	45.44	18.75	17.39
SWNT-0.05%	36.87	8.26	-4.75
SWNT-0.5%	49.89	17.00	28.89
CdS-0.05%	43.81	9.43	13.18
CdS-0.5%	37.09	8.54	-4.19

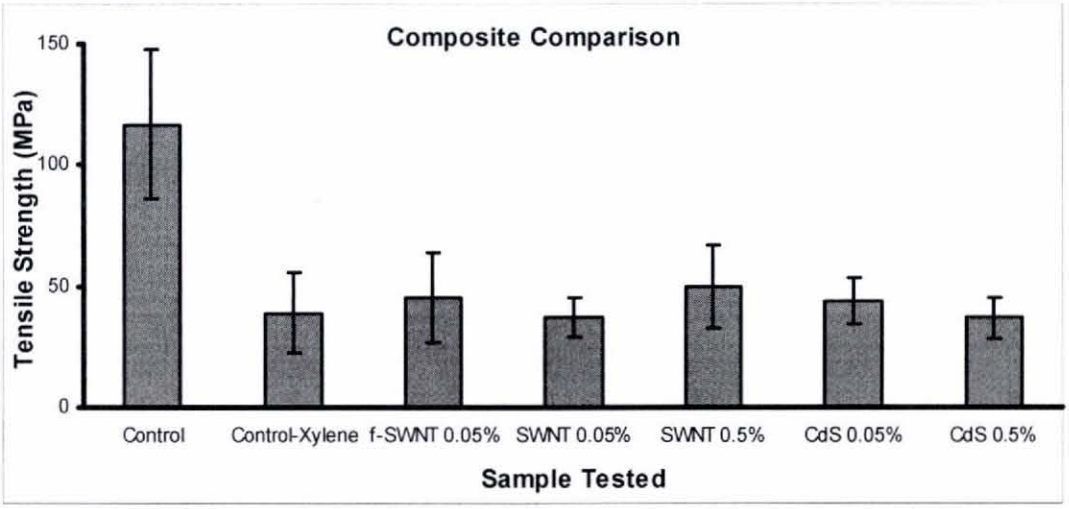

Figure 4.9: Comparison of tensile strength

Table 4.11 shows the stiffness of the nanocomposites all degraded compared to the pristine control sample. SWNT-0.05% and SWNT-0.5% degraded 38% and 15%, respectively. The stiffness of f-SWNT reduced 5%. CdS-0.05% and CdS-0.5% stiffness degraded 30% and 20%, respectively. However, if the SWNT samples were compared to the processed control-xylene sample, table 4.12 and figure 4.10 show the stiffness increased with the addition of nanomaterials. The

addition of 0.05%wt. and 0.5%wt. SWNT increased stiffness by 6.0% and 47%, respectively. Similarly, CdS concentrations of 0.05%wt. and 0.5%wt. had their stiffness values increased 21% and 32%, respectively. There was a stiffness gain of 51% in f-SWNT compared to the same concentration of pristine SWNT, with an overall stiffness increase of 63% as compared to the CX sample.

Table 4.11: Comparison of stiffness relative to control

Sample	Young's Modulus (MPa)	Standard Deviation	% Difference
Control	224.77	112.03	0.00
Control-Xylene	130.72	44.30	-41.84
f-SWNT-0.05%	213.72	92.83	-4.91
SWNT-0.05%	139.09	21.98	-38.12
SWNT-0.5%	191.68	60.73	-14.72
CdS-0.05%	158.22	29.46	-29.61
CdS-0.5%	180.08	27.56	-19.88

Table 4.12: Comparison of stiffness relative to control-xylene

Sample	Young's Modulus (MPa)	Standard Deviation	% Difference
Control	224.77	112.03	71.94
Control-Xylene	130.72	44.30	0.00
f-SWNT-0.05%	213.72	92.83	63.49
SWNT-0.05%	139.09	21.98	6.40
SWNT-0.5%	191.68	60.73	46.63
CdS-0.05%	158.22	29.46	21.03
CdS-0.5%	180.08	27.56	37.76

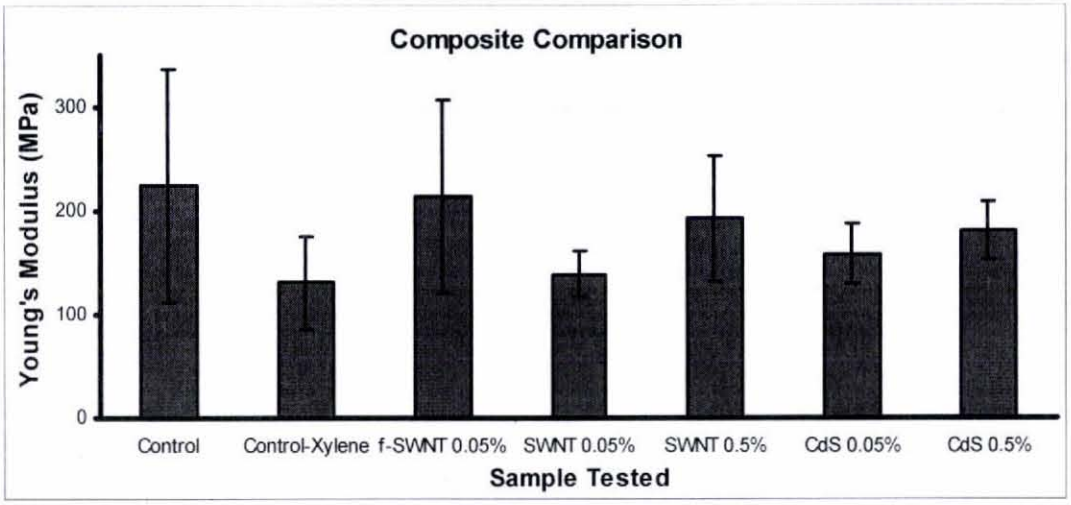

Figure 4.10: Comparison of stiffness

Table 4.13 show the strain to failure of most of the nanocomposites all degraded compared to the pristine control sample, except for f-SWNT-0.05% and CdS-0.5% which experienced an increase of 14% and 10% respectively. SWNT 0.05%wt. and 0.5%wt. degraded by 52% and 13%, respectively. The strain to failure of CdS-0.05% degraded 27%. However, if the samples were compared to the processed control-xylene sample, table 4.14 and figure 4.11 show the strain to failure values increased with the incorporation of nanomaterials. Between the SWNT concentrations of 0.05%wt. and 0.5%wt., the strain to failure values increased 25.4% and 128%, respectively. However, with functionalization, a strain to failure of 2.77 was obtained, a 199% increase. Functionalization also increased strain to failure by 139% as compared to the same concentration of pristine SWNT. The cadmium sulfide nanoparticle concentration of 0.05%wt. yielded an increase of 91%. At 0.5%wt. of CdS, a strain to failure increase of 188% was achieved.

Table 4.13: Comparison of strain to failure relative to control

Sample	Strain to Failure	Standard Deviation	% Difference
Control	2.42	0.82	0.00
Control-Xylene	0.93	0.20	-61.77
f-SWNT-0.05%	2.77	0.56	14.23
SWNT-0.05%	1.16	0.13	-52.05
SWNT-0.5%	2.11	0.37	-12.78
CdS-0.05%	1.77	0.36	-27.13
CdS-0.5%	2.67	0.37	10.27

Table 4.14: Comparison of strain to failure relative to control-xylene

Sample	Strain to Failure	Standard Deviation	% Difference
Control	2.42	0.82	161.59
Control-Xylene	0.93	0.20	0.00
f-SWNT-0.05%	2.77	0.56	198.80
SWNT-0.05%	1.16	0.13	25.43
SWNT-0.5%	2.11	0.37	128.16
CdS-0.05%	1.77	0.36	90.63
CdS-0.5%	2.67	0.37	188.45

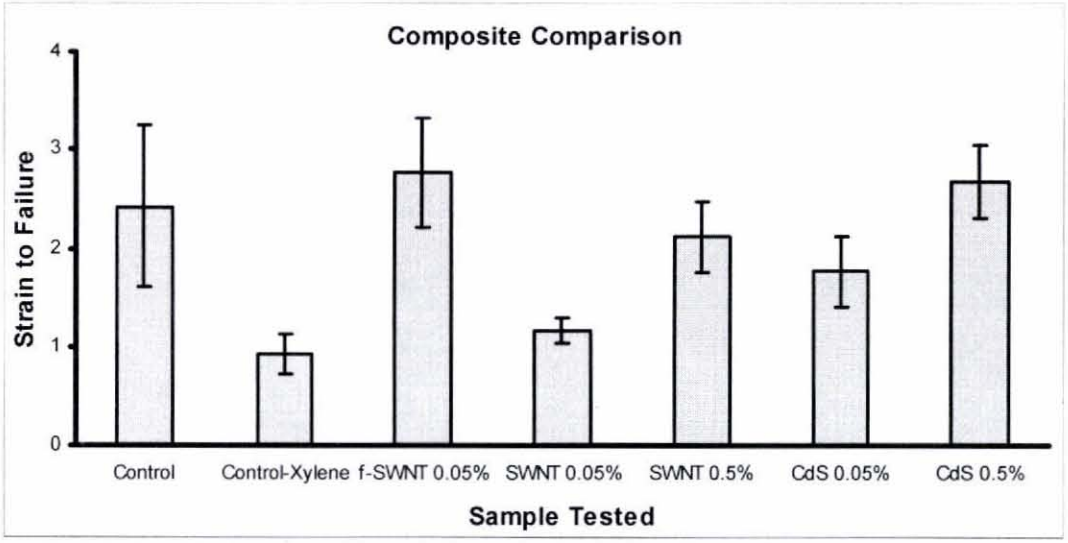

Figure 4.11: Comparison of strain to failure

Table 4.15 shows the toughness of the nanocomposites all degraded compared to the pristine control sample. SWNT 0.05%wt. and 0.5%wt. degraded by 89% and 66%, respectively. The toughness of f-SWNT reduced 55%. CdS-0.05% and CdS-0.5% toughness experienced a degradation of 75% and 66%, respectively. However, if the composites were compared to the processed control-xylene sample, table 4.16 and figure 4.12 show the toughness values increase in nanoparticle concentrations. Pristine SWNT at 0.05%wt. and 0.5%wt. produced toughness values 8.0% and 200% greater than CX values, respectively. Functionalization of 0.05%wt. SWNT achieved an increase of 301%. Compared to the same concentration of pristine SWNT, functionalized SWNT yielded 273% increase. The 0.05%wt. and 0.5%wt. CdS nanocomposites experienced a toughness increase of 124% and 199%, respectively.

Table 4.15: Comparison of toughness relative to control

Sample	Toughness (MJ/m^3)	Standard Deviation	% Difference
Control	257.68	170.60	0.00
Control-Xylene	29.09	21.19	-88.71
f-SWNT-0.05%	116.74	62.87	-54.69
SWNT-0.05%	31.32	3.83	-87.85
SWNT-0.5%	87.14	32.14	-66.18
CdS-0.05%	65.09	11.71	-74.74
CdS-0.5%	87.09	22.89	-66.20

Table 4.16: Comparison of toughness relative to control-xylene

Sample	Toughness (MJ/m^3)	Standard Deviation	% Difference
Control	257.68	170.60	785.69
Control-Xylene	29.09	21.19	0.00
f-SWNT-0.05%	116.74	62.87	301.26
SWNT-0.05%	31.32	3.83	7.65
SWNT-0.5%	87.14	32.14	199.53
CdS-0.05%	65.09	11.71	123.74
CdS-0.5%	87.09	22.89	199.35

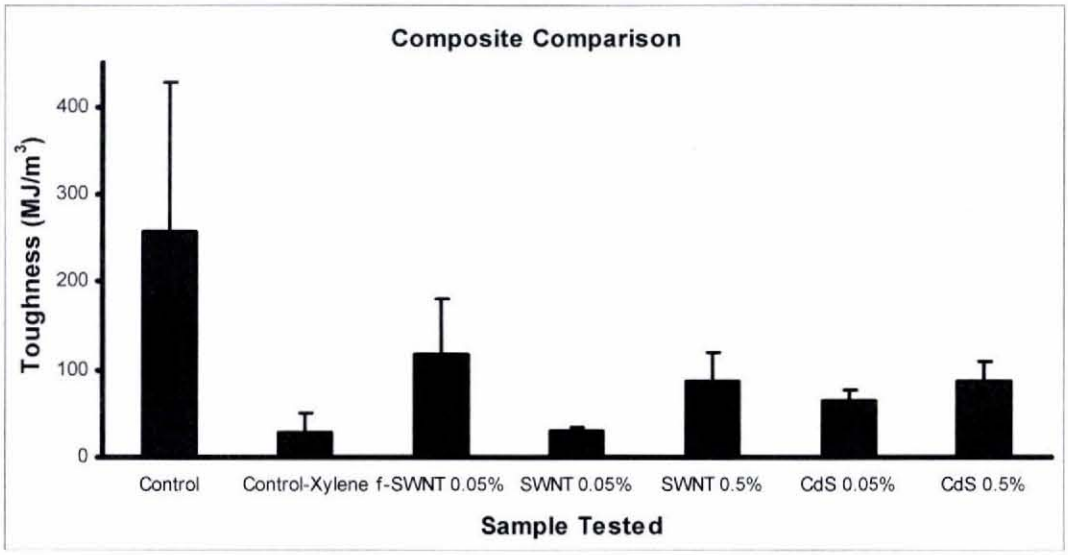

Figure 4.12: Comparison of toughness

CHAPTER 5

DISCUSSION AND CONCLUSION

Based on the gathered data, the effects on the incorporation of the various nanomaterials and their varying concentrations were discussed. As well as, overall conclusions on the methods used such as in the processing procedure and monofilament fabrication. There are critical assumptions and points made throughout the experiment which would introduce errors into the results, such as the large load cell and strain and cross-sectional measurement methods. Nevertheless, based on the obtained results, conclusions were made on the use of nanomaterials to reinforce polymers, particularly the benefits of using functionalized CNT.

5.1 Effects of Nanomaterial Incorporation

Compared to the nanocomposite materials subjected to xylene exposure, the pristine control LDPE sample had superior performance in tensile strength, stiffness, and toughness. However, strain to failure increased to some degree with the incorporation of f-SWNT-0.05% and CdS-0.5%.

The processing method required the use of xylene, a good solvent for LDPE, to incorporate the nanomaterials. However, even with vacuum pumping to remove and evaporate the solvent out of the polymer matrix its effects still remain. The use of xylene to process the material severely degraded the overall properties of the polymer, as evident in the control and control-xylene results. However, if the

control-xylene sample is the basis for comparison of the nanocomposites, we see improvements in the investigated material properties. Tensile strength increased from 38.7 MPa to 45.4, 49.89, and 43.81 MPa for f-SWNT-0.05%, SWNT-0.5%, and CdS-0.05% respectively. Stiffness increased from 130.72 MPa to 213.72, 139.09, 191.68, 158.22, and 180.08 MPa for f-SWNT-0.05%, SWNT-0.05%, SWNT-0.5%, CdS-0.05%, and CdS-0.5% respectively. Strain to failure increased from 0.93 to 2.77, 1.16, 2.11, 1.77, and 2.67 for f-SWNT-0.05%, SWNT-0.05%, SWNT-0.5%, CdS-0.05%, and CdS-0.5% respectively. Toughness increased from 29.09 MPa to 116.74, 32.32, 87.14, 65.09, and 87.09 MPa for f-SWNT-0.05%, SWNT-0.05%, SWNT-0.5%, CdS-0.05%, and CdS-0.5% respectively.

5.2 Effects of Nanomaterial Concentration

The addition of more nanomaterials tends to increase the measured material properties. As seen by adding 0.05%wt. and 0.5%wt. SWNT, there's an increase in strength, stiffness, strain to failure, and toughness. Carbon nanotubes are known to have high strength, stiffness so as expected these characteristics are a direct correlation to the increased strength and stiffness of the composite material. The increase in toughness could be due to the detour of micro-crack propagation caused by nanotubes embedded in polymer matrix. Increased toughness helps to explain the increased strain to failure. Toughness being the integral of the stress-strain curve, increased strain to failure, as well as strength, results in higher toughness values.

Functionalizing the SWNT makes a significant difference in the composite's overall performance. Strength, stiffness, strain to failure, and toughness were all improved by 23%, 51%, 139%, and 273%, respectively, compared to the same concentration of SWNT. Functionalizing the SWNT changes its surface allowing it to bond better to the polymer matrix and promote dispersion of nanotubes in LDPE. The effects of an improved interface between filler and matrix, allow the load to be transferred from the matrix to the nanotubes.

Not much is known about the mechanical attributes of cadmium sulfide nanoparticles. Their primary use has been to enhance optical properties. However, CdS-0.5% performed almost as well as f-SWNT-0.05% in all measured properties. The CdS nanoparticles serve as filler reinforcing the polymer matrix. Just as with the increasing SWNT concentrations, the trend of adding more CdS also increased the material's stiffness, strain to failure, and toughness. However, the tensile strength from CdS-0.05% to CdS-0.5%, reduced by15%.

More samples at varying concentrations for each type of nanomaterial would provide a more complete picture. However, due to time and material availability constraints this study was limited to just aforementioned composites and their respective concentration levels. Increasing nanomaterial concentrations is expected to increase material properties up to a certain optimal point, after which, the composites get overwhelmed and start to degrade.

5.3 Conclusion

The initial objectives of this study have been met. A simple method of producing continuous (meter-scale) LDPE nanocomposite monofilaments of relative consistency was developed. The samples were tested for their mechanical properties and information was obtained about incorporating various nanomaterials at various concentrations, as well as, the effect of functionalization. Additional information on the effect of the processing method itself was also obtained.

Using the thermoplastic behavior of LDPE, the bulk material was melted down to draw out continuous lengths of LDPE monofilaments with diameters on the micron range, and lengths several meters long. The novel method had little control over the cross-section so broad assumptions were made which undoubtedly influenced the results, but should give a general representation of the relative mechanical behavior between samples.

The processing method revealed some drawbacks. Using organic solvents to incorporate the nanomaterials ended up weakening the material, as seen by comparing the pristine control sample to the processed control-xylene sample. Strength, stiffness, strain to failure, and toughness all reduced by 67%, 42%, 61%, and 89% respectively. Given more time and resources, increased concentrations of nanomaterials may produce better results, as initially indicated by the two concentrations tested. They may even surpass the properties of the pristine control sample.

Being that this study is purely relative, the benefits of incorporating nanomaterials as a means to increase material properties were shown by comparing the processed LDPE without nanomaterials (CX), with its nanocomposite counterparts, f-SWNT, SWNT, and CdS. Most nanomaterial tested showed an improvement in strength, stiffness, strain to failure and toughness. An improvement of 17% in tensile strength was shown by f-SWNT-0.05%; a similar increase was also shown for the cadmium sulfide sample. Functionalized SWNT also showed the greatest improvements in stiffness, strain to failure, and toughness at 63%, 199%, and 301% respectively; followed closely by the improvements shown with 0.5%wt. CdS.

It is evident that functionalization of SWNTs make a significant difference in the performance of the composites. As mentioned previously, increasing concentrations also aid in increasing material properties. Various other nanomaterials can also potentially achieve the same goal as the much acclaimed carbon nanotube. Cadmium sulfide nanoparticles appear to reinforce composite materials, even though they are more commonly used for their optical properties.

Based on the findings of this study, a conclusion can be drawn for the processing method, and effects of adding various nanomaterials at various concentrations. The processing method of incorporating nanomaterials into LDPE used in this study will initially weaken the material. However, the benefits of incorporating nanomaterials as a means to increase material properties were shown

by comparing the processed control-xylene sample, which had no nanomaterials, with its nanocomposite counterparts. Increasing the nanomaterial concentration appeared to increase strength, stiffness, strain to failure, and toughness. Functionalizing SWNT significantly improves the performance of the composite compared to using pristine SWNT. Cadmium sulfide nanoparticles can also reinforce composite materials, even though they are more commonly used for their optical properties.

These results show a promising effect in the addition of nanomaterials to increase material properties in composite materials. However, further work would involve improving the processing method, and optimizing the loading percentage of nanomaterials in the composites. Additional work, including various nanomaterials, like MWNT, as well as, the mechanical attributes of CdS and other zero-dimension nanoparticles will aid in the advancement of the field.

APPENDIX A

PREVIOUS RESEARCH PROJECTS

Epoxy-Composite Casting

Creating and testing epoxy/CNT composite molds was one of the first areas researched. However, properly dispersing the CNTs into the epoxy remained a major obstacle. CNTs tend to aggregate and clump together when mixed with most liquids. The non-uniform dispersion becomes a material flaw and weakens the composite. One way of transferring the CNTs into the epoxy used solvent as a means to thin out the viscosity of epoxy and disperse the CNTs. The solvents tried were acetone and ethanol alcohol. The CNTs were first sonicated in the solvent, dispersing them fairly well, then the solvent/CNT were mixed with the epoxy resin (part "A") before mixing in the hardener (part "B"). The ratios of solvent to part "A" and part "A" to "B" were 1:1, and 1:3 respectively.

The resulting composites were very flexible, although homogeneous dispersion seemed to be achieved. However, based on the control samples the flexibility was due majority to the epoxy's reaction with the solvent. To solve this problem the "A"/solvent/CNT solution were mixed on a hot plate and weighed periodically until the solvent weight evaporated. This method appears to reduce the effect of the solvent yet still achieving a homogenous composite, however, it is still

hard to determine if all of the solvent's influence has been removed, and the remaining effects is purely due to the CNTs.

Epoxy-Composite Ropes

Following in the footsteps of the cast composites, composite ropes were made. Individual strands were drawn out from a curing epoxy/CNT solution. With the strands connected at one end, the other ends shared the tip of a small electric motor and spun. However, many problems were encountered by this method. Aggregation of the CNTs and solvent influence aside; sample repeatability, including strand diameters and twist angles, as well as consistent diameters throughout the rope were other issues, see Figure A.1. Samples were also very difficult to make. Strands could only be drawn out a few inches, and needed to be twisted within a specific frame, too early and the strands melt together, too late and the strands are too brittle for twisting. The time involved for such limited and inconsistent samples seemed very impractical, and the project put on hold.

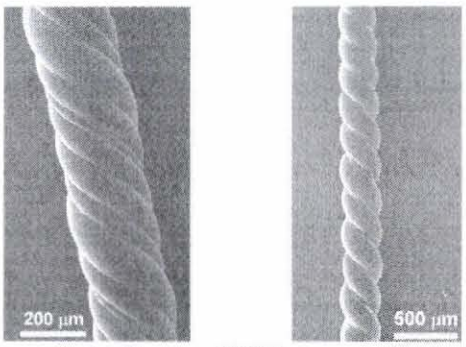

Figure A.1: Epoxy-CNT composite twists

Epoxy-Composite Thin Films

The next project involved making epoxy-nanocomposite thin films. Preparation of the materials remained similar to previous methods, but instead of pulling out strands of epoxy to make ropes, bubbles were blown in the same manner a child blows bubbles with soap and water. Sections of the bubbles were taken as thin film composites and tested for CNT composition. It is interesting to note the surface tension while blowing the bubbles appears to physically align the dispersed CNTs [13]. It is being researched further.

Impact Analysis of Aligned CNT Films

The next studies strayed away from composite materials and investigated purely the CNT film as grown in the furnace. Impact tests comprised of testing only the aligned, "as-grown" CNT films. Steady loading of CNTs in the axial direction are well-documented, contrary to the behavior of CNTs under dynamic impulsive loadings. The method we considered would simply use a dropping ball, and the effects later examined under a scanning electron microscope.

However, previous studies exhibited the CNTs resilience and resistance to deformation. The exact behavior during impact would therefore be unknown by our methods, only the ending deformation. Other studies used a piezoelectric gauge to measure the contact force in real time, [29-30]. The force-time curve then converted into a force-displacement curve via conservation of linear momentum. Based on prior research, it's plausible to say that our method of testing and then

measuring, instead of measuring while testing, would be insufficient for accurate results. Unless many tests at varying impact velocities can be done on identical CNT films to locate when buckling occurs, advancement on the project with the equipment currently available will be postponed.

Lateral Compression of Aligned CNTs

Much work has been done on axial tension and compression of CNTs, but compression on the lateral/transverse direction (see Figure A.2) hasn't been studied as much. Most literature used theoretical numerical modeling or very expensive, innovative techniques to test the CNT films on the micro/nano scale to obtain their property values, [32, 38, 47-48].

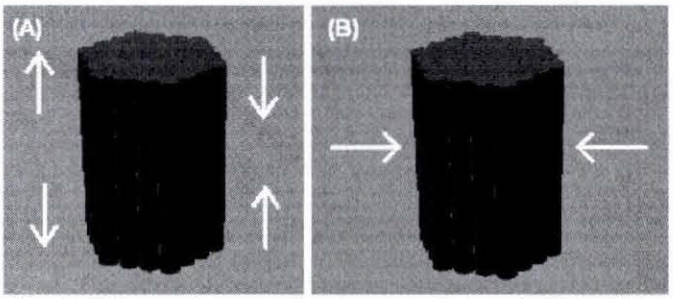

Figure A.2: (A) Axial tension and compression of CNT bundle, (B) lateral compression of CNT bundle.

Our method would be testing on the macro scale. This would require growing extra long CNTs to be put into the mechanical testing machine we have available. Testing on a larger scale would seem more practical if CNTs are to be grown in bulk and applied in large scale applications. Previous studies, while useful in verifying theoretical values test only a single CNT or use very short

samples. However, the first step would be to grow very long CNTs, preferably over 5mm. Much time has gone into varying the CVD parameters with the means we have to make it better, but no improvements were made. Our current method compared to previous literature, which used a thermo-mechanical analyzer and SEM manipulation, may not be up to the same caliber in accuracy, but still could be interesting to see how it compares.

Compression Tests on CNT Pillars, (M.I.T. Collaboration):

We provided some assistance to a project in collaboration with Professor Onnik Yaglioglu of Massachusetts Institute of Technology and FormFactor Inc. in California. Patterned samples were sent to us to grow pillars of CNT. The patterns were formed by sputtering a gold film onto masked SiO_2 wafers; see Figure A.3(a). Removing the masked sections revealed the bare substrate where the CNTs could adhere and grow; see Figure A.3(b). Consistency and control in sample length became an important issue. The tested samples varied in height and cross-section geometry, see Figure A.3(c) and A.3(d). Axial compression loads were applied to the pillars to investigate their mechanical properties, particularly their buckling characteristics. Recent results exhibited buckling in various locations from the bottom to middle of the pillars. Possible explanations lie in the interaction of CNTs on the substrate and catalyst nucleation.

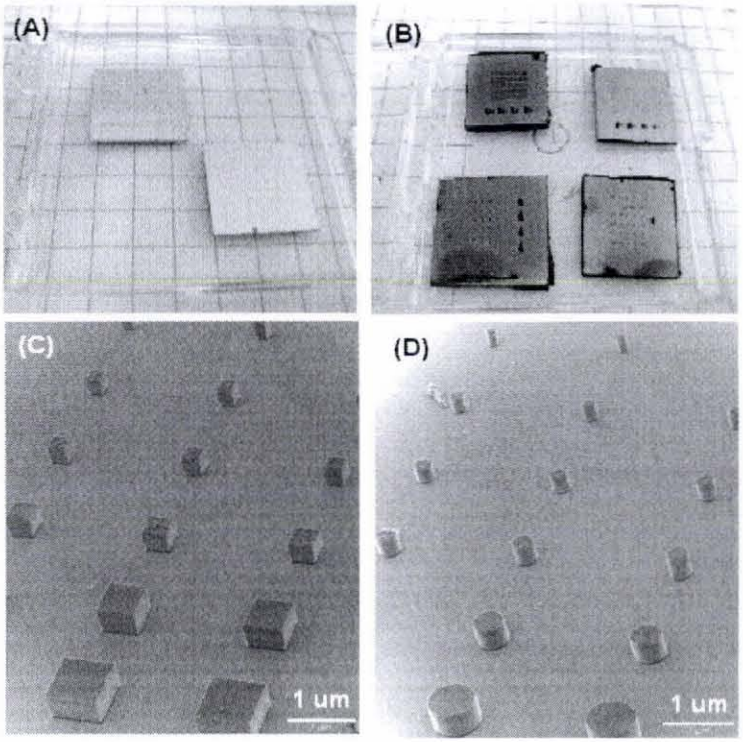

Figure A.3: (A) Gold sputtered pattern on SiO2 wafer, (B) SiO2 wafer with CNT growth, (C) and (D) SEM images of patterned CNT growth.

Nylon 6,10-CNT Composite Yarns

Nylon, a.k.a polyamide (PA), is a general name for a family of synthetic polymers formed by repeating molecular units linked by peptide (amide) bonds. Nylons are the product of reacting equal parts of a diamine and dicarboxylic acid. Classification of nylons involve numerical suffixes, the first number and second number denote the number of carbons donated by the diamine and diacid respectively. Nylon 6,6 is the most common grade of nylon. Compared to PA66,

PA610 is weaker and more expensive; however, they hold their properties better under lower temperatures and have lower moisture absorption.

The basis of the experiment is a popular chemistry demonstration mixing two solutions and drawing out a nylon thread from the interface. Solution "A" consists of 0.5M of hexamthylene diamine, a.k.a 1,6-diaminohexane ($H_2N(CH_2)_6NH_2$), and 0.5M of sodium hydroxide in water. Solution "B" consists of 0.2M of sebocoyl chloride ($ClOC(CH_2)_8COCl$) in hexane. A 1 to 1 ratio of solutions "A" and "B" are poured separately into the same jar, the organic layer ("B") sits on top of the aqueous layer ("A"). The reaction at the solution interface can be hooked and the solidifying threads wound onto a spool. The process is called interfacial polymerization, see figure A.4 below.

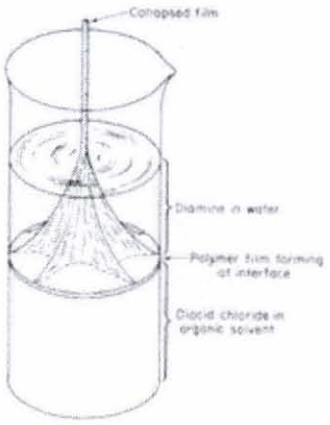

Figure A.4: Interfacial polymerization of nylon 6,10, [24]

The inclusion of CNTs was to be within the aqueous layer dispersing them into the solution by chemical functionalization. Sodium dodecyl sulfate, a surfactant similar to soap, will aid in the dispersion of CNTs into the aqueous

solution. Control samples without CNTs was also to be made to test for comparison

There was little control over the cross-section of the fibers, and they were very weak, salt crystals and gaps were prevalent in the drawn out yarn. Subsequent rinsing, melting and extrusion was attempted to normalize the material. Figure A.5 shows the instrument setup. Nylon 6,10 would oxidize before reaching its melting temperature so an inert gas, argon, was pumped through the system as a Bunsen burner melted the bulk nylon 6,10 material in a glass syringe. Upon melting, the syringe plunger was to extrude the material into a water bath. However the material was too viscous to be extruded by the means on this setup. As a result, this study was terminated.

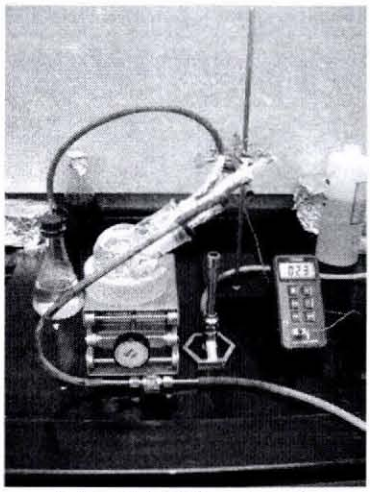

Figure A.5: PA610 extrusion setup

APPENDIX B

COMPLETE SET OF SEM IMAGES

Control Specimens

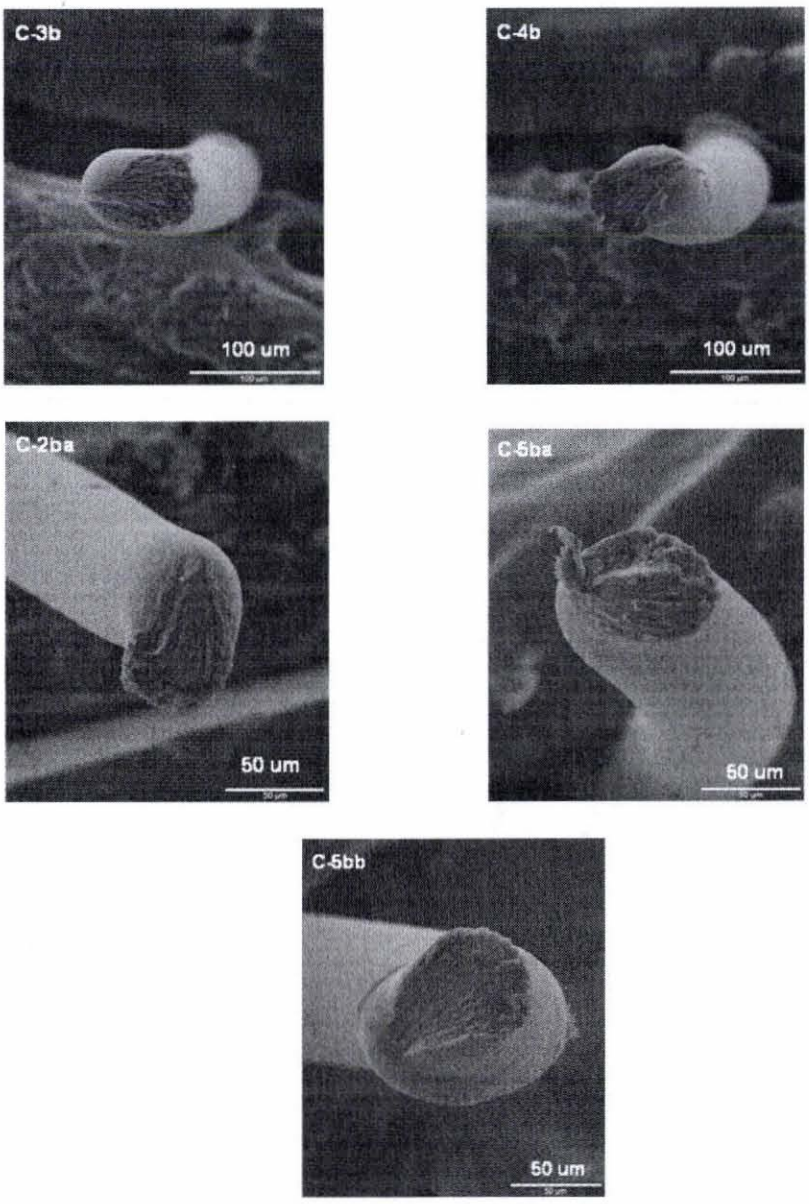

Figure B.1: SEM of control specimens: C-3b, C-4b, C2ba, C-5ba, C-5bb

Control-Xylene Specimens

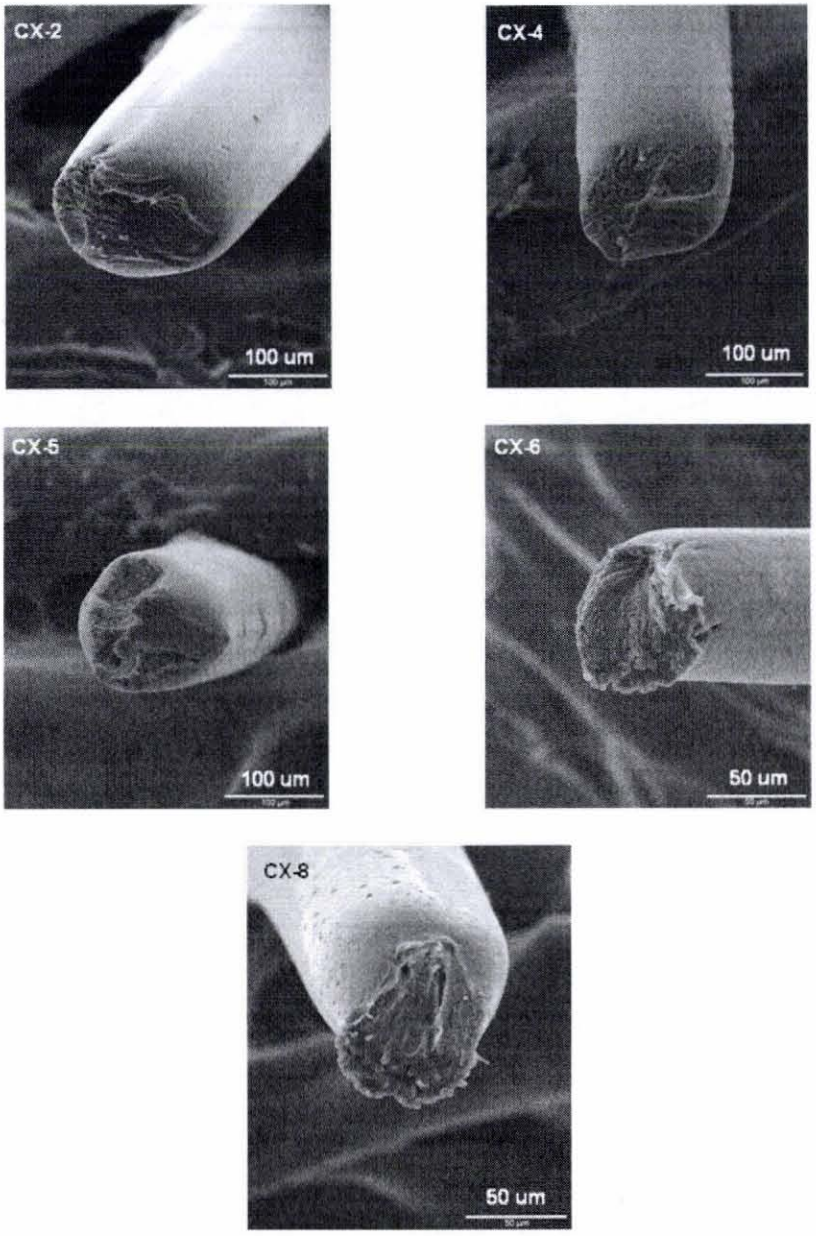

Figure B.2: SEM images of control-xylene specimens: CX-2, CX-4, CX-5, CX-6, and CX-8

Functionalized Single-Wall Carbon Nanotubes, 0.05% wt.

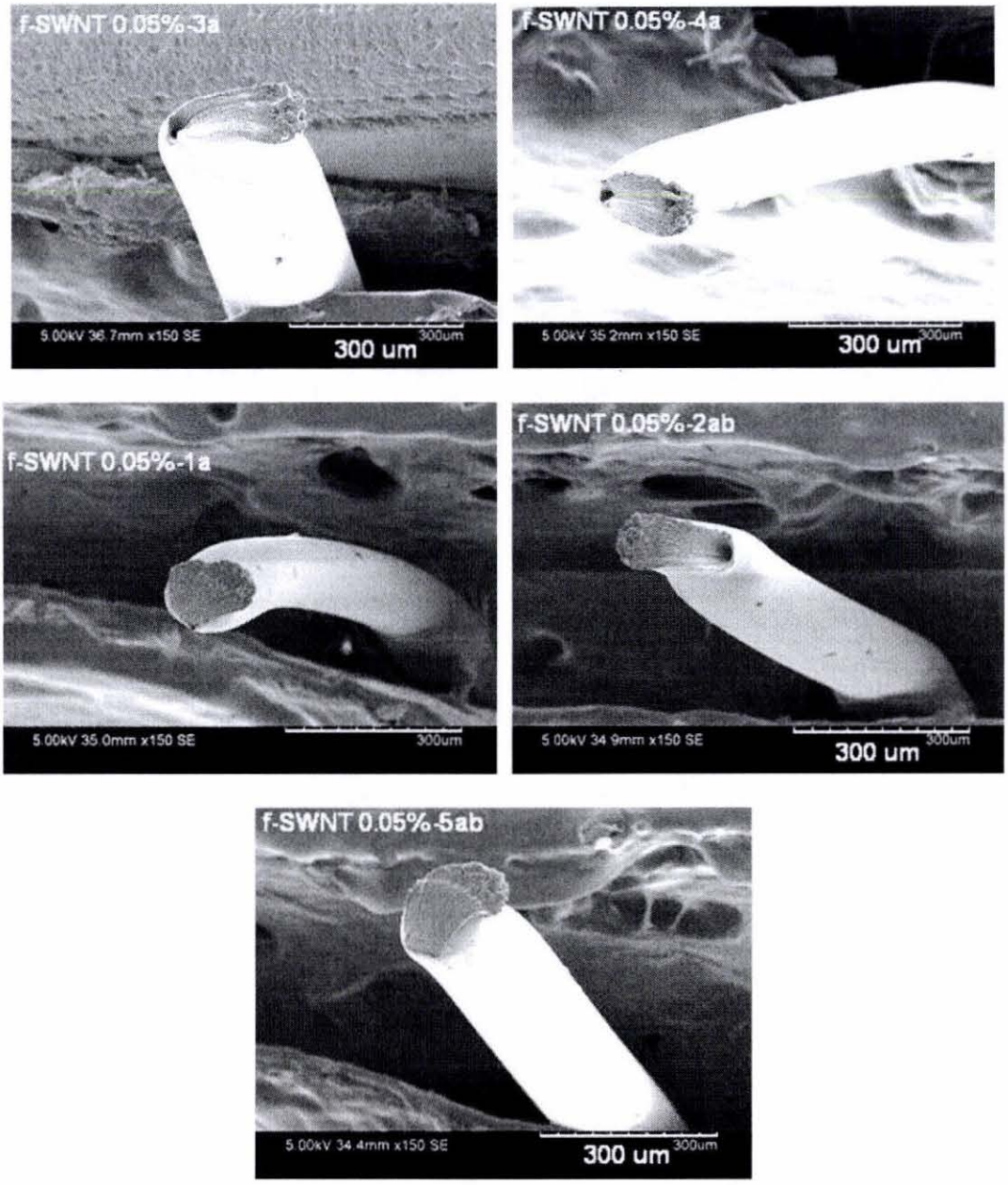

Figure B.3: SEM images of f-SWNT 0.05% wt. specimens: f-SWNT-0.05%-3a, f-SWNT-0.05%-4a, f-SWNT-0.05%-1a, f-SWNT-0.05%-2ab, f-SWNT-0.05%-5ab.

Single-Wall Carbon Nanotubes, 0.05% wt.

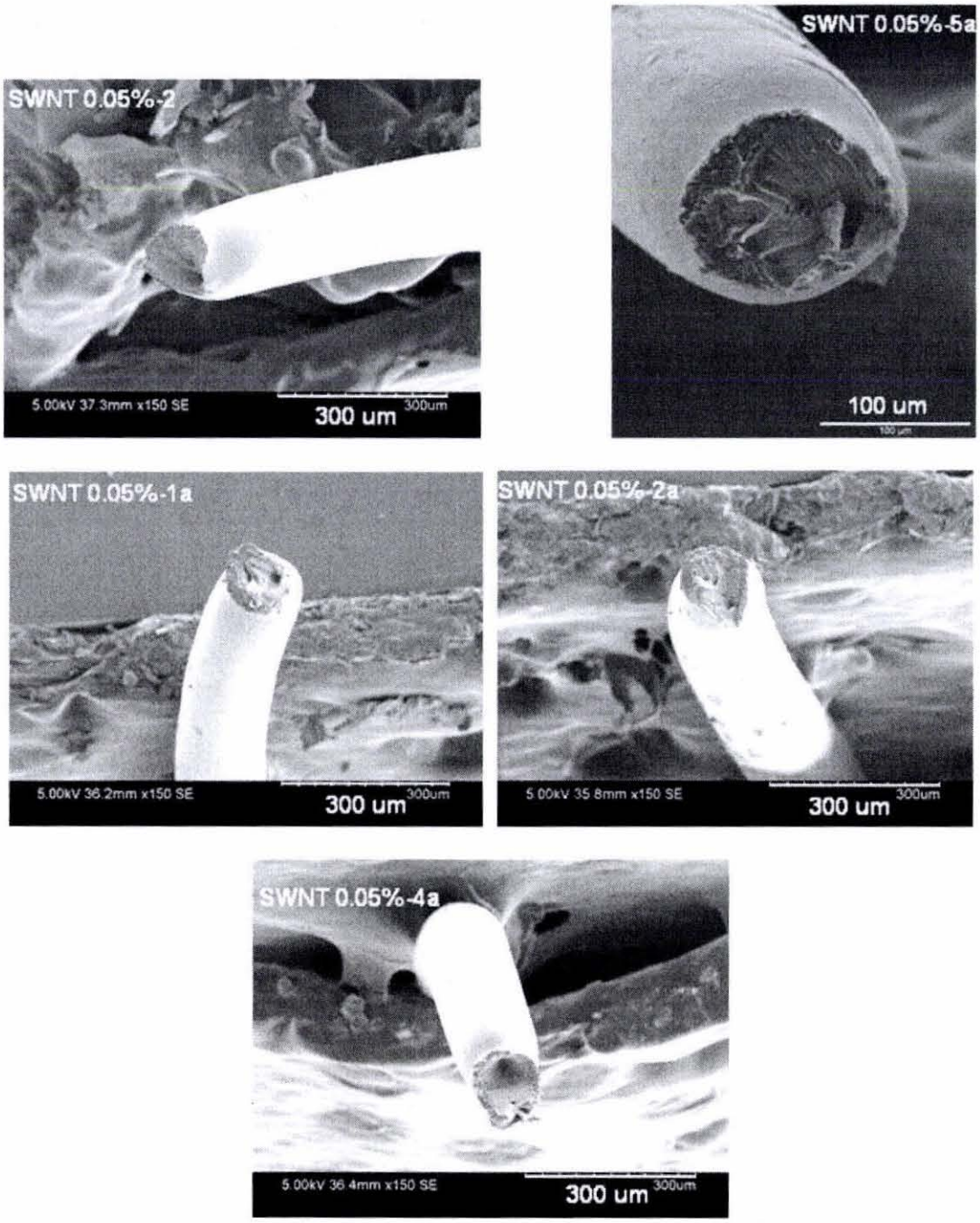

Figure B.4: SEM images of SWNT 0.05% wt. specimens: SWNT-0.05%-2, SWNT-0.05%-5a, SWNT-0.05%-1a, SWNT-0.05%-2a, SWNT-0.05%-4a.

Single-Wall Carbon Nanotubes, 0.5% wt.

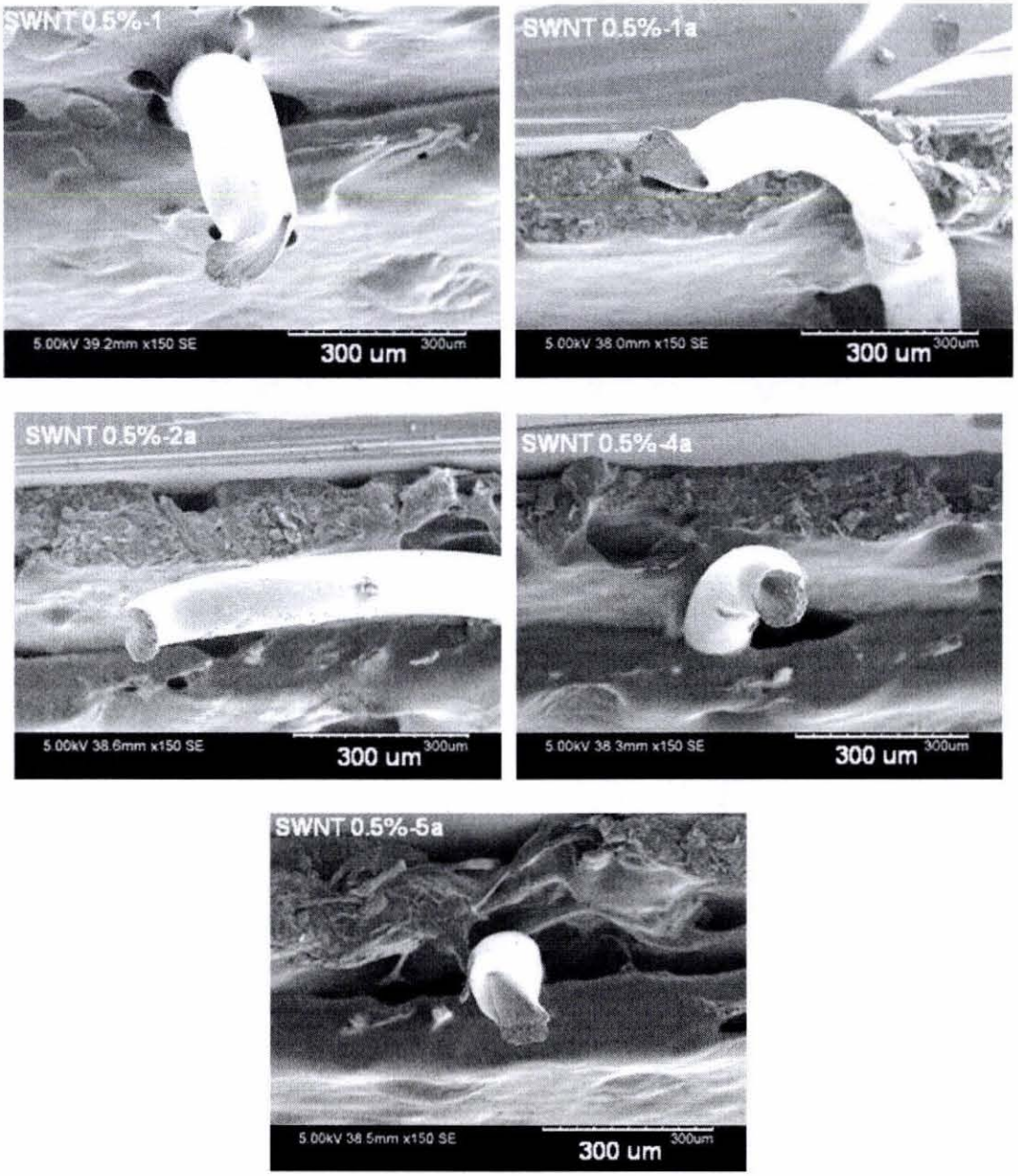

Figure B.5: SEM images of SWNT 0.5% wt. specimens: SWNT-0.5%-1, SWNT-0.5%-1a, SWNT-0.5%-2a, SWNT-0.5%-4a, SWNT-0.5%-5a.

Cadmium Sulfide Nanoparticles, 0.05% wt.

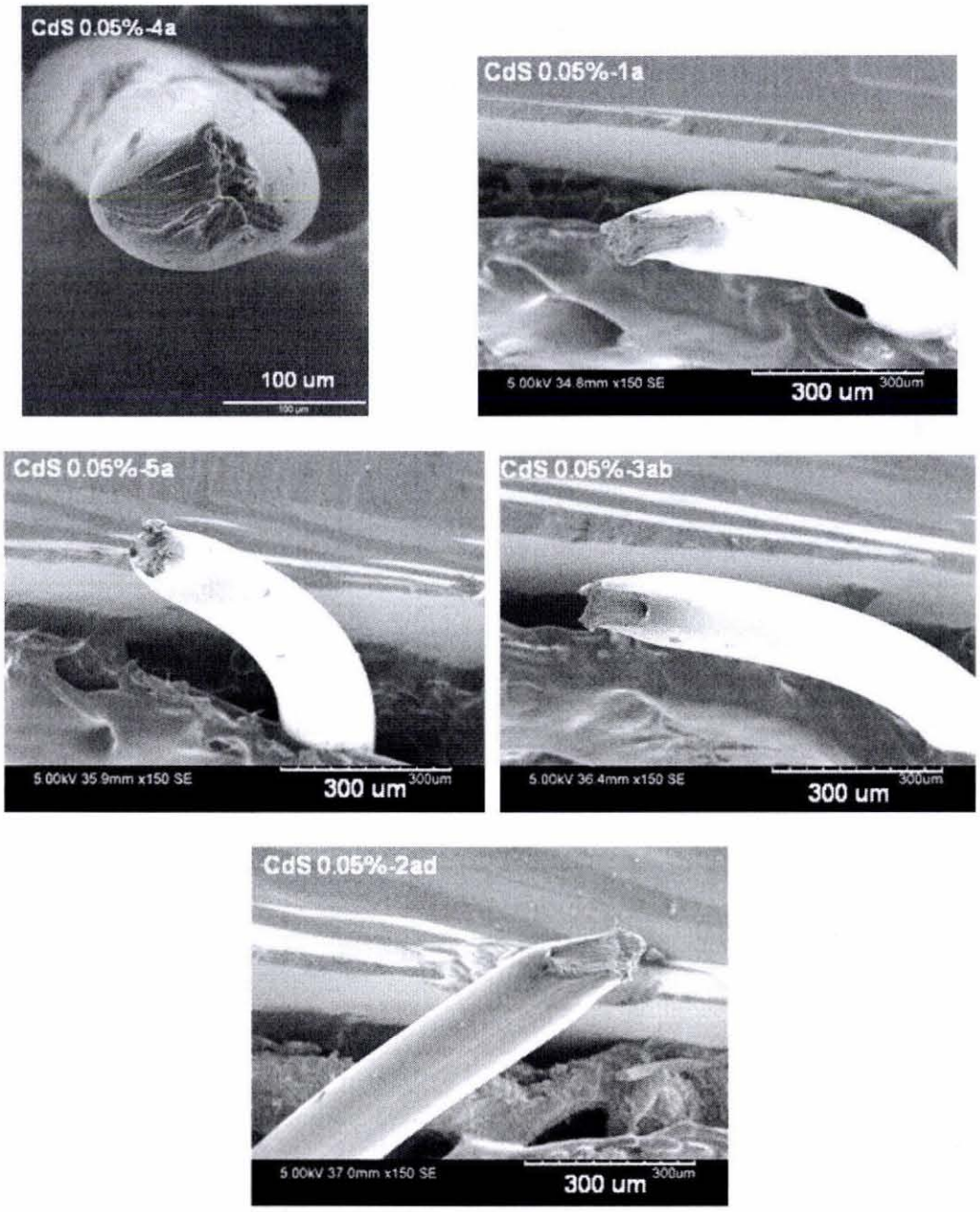

Figure B.6: SEM images of CdS 0.05% wt. specimens: CdS-0.05%-4a, CdS-0.05%-1a, CdS-0.05%-5a, CdS-0.05%-3ab, CdS-0.05%-2ad.

Cadmium Sulfide Nanoparticles, 0.5% wt.

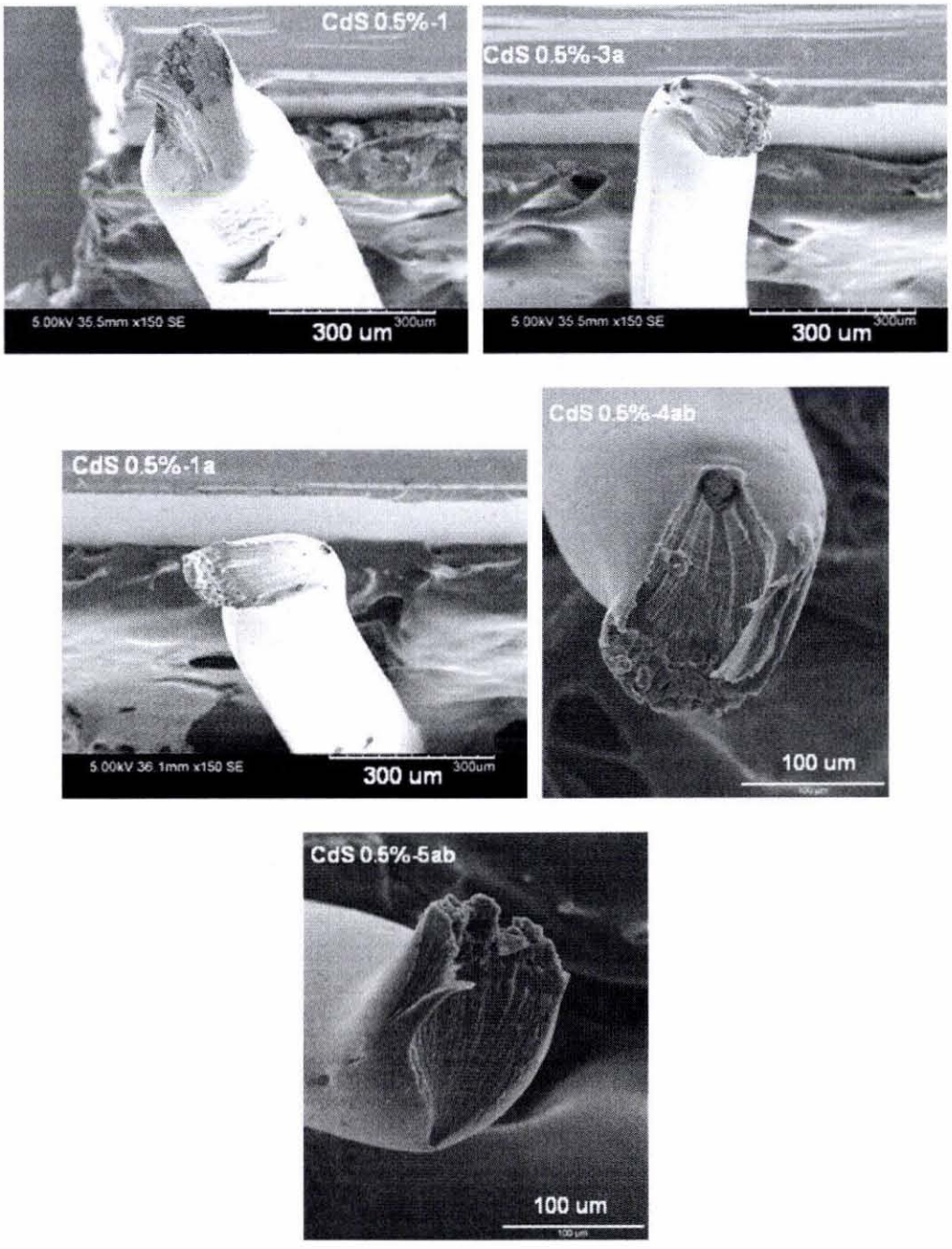

Figure B.7: SEM images of CdS 0.5% wt. specimens: CdS-0.5%-1, CdS-0.5%-3a, CdS-0.5%-1a, CdS-0.5%-4ab, CdS-0.5%-5ab

APPENDIX C

INSTRON RAW DATA REPORTS

Raw Data: Control

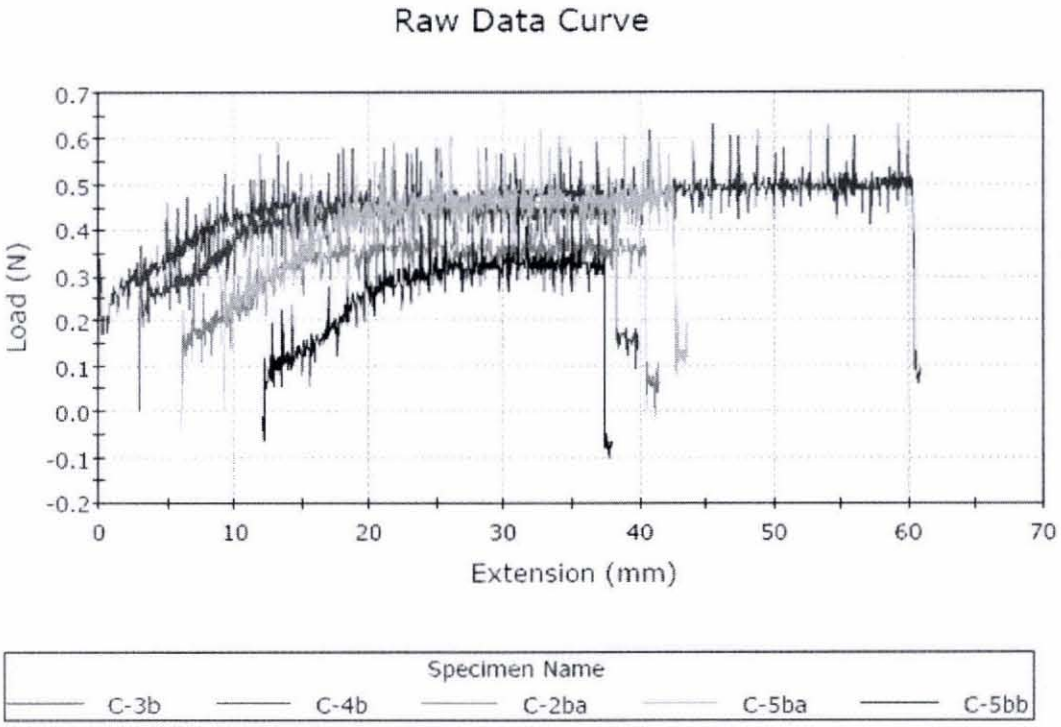

Figure C.1: Load-extension curve for control sample.

Table C.1: Control sample raw data

Raw Data

	Load at Machine Peak Load (N)	Extension at Break (Standard) (mm)
15	0.63174	60.91800
16	0.59232	36.91880
19	0.51328	35.51070
22	0.63174	34.68020
25	0.47386	25.78130

Material Properties Data: Control

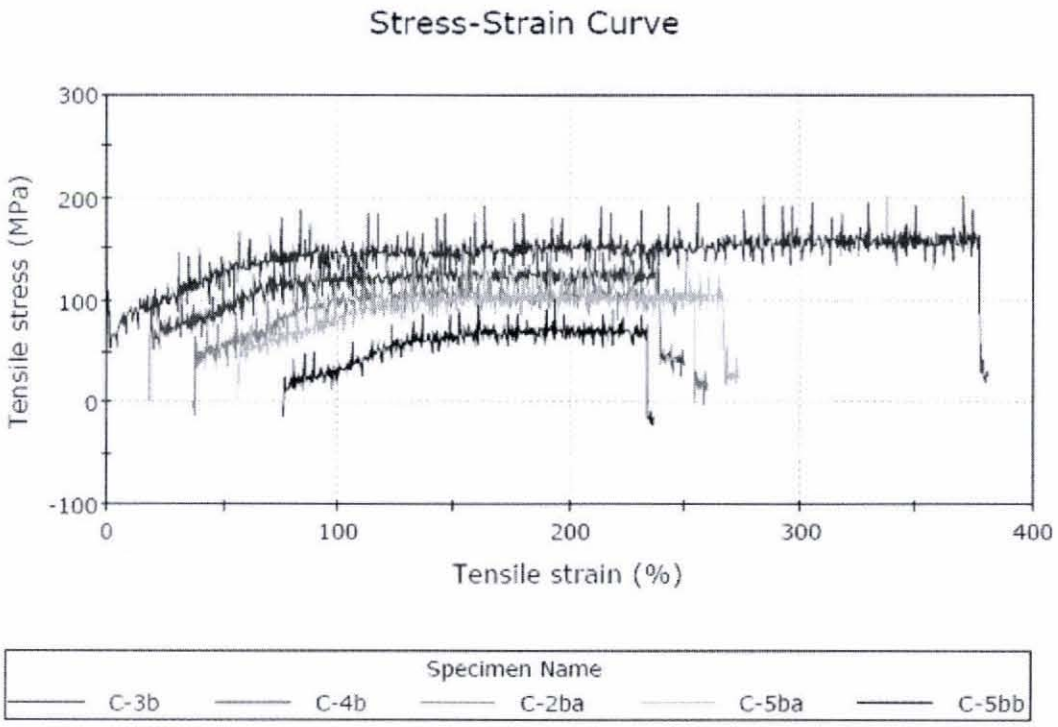

Figure C.2: Stress-strain curve for control samples.

Table C.2: Control sample material properties data.

Property Values

	Tensile stress at Tensile Strength (MPa)	Tensile strain at Break (Standard) (mm/mm)	Modulus (Young's 0 mm - 10 mm) (MPa)
15	167.14891	3.80737	406.11176
16	120.98510	2.30743	198.63882
19	105.90055	2.21942	247.69832
22	103.91608	2.16751	124.73580
25	86.63582	1.61133	146.65762

Raw Data: Control-Xylene

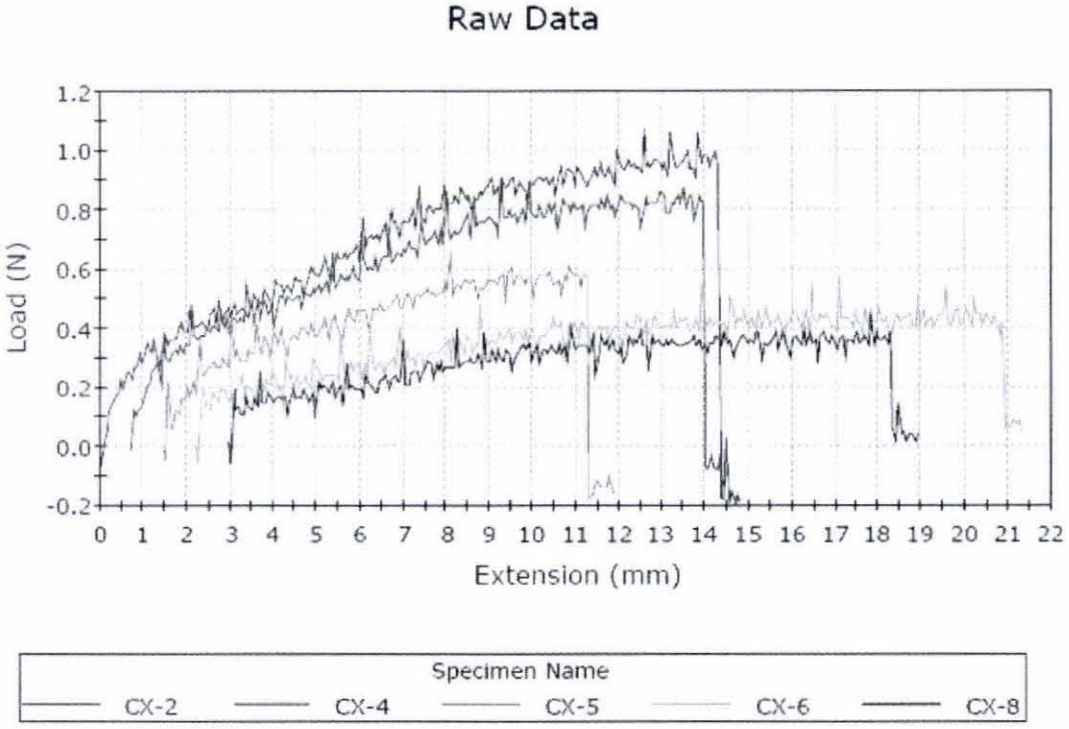

Figure C.3: Load-extension curve for control-xylene sample.

Table C.3: Control-xylene sample raw data

Raw Data

	Load at Machine Peak Load (N)	Extension at Break (Standard) (mm)
2	1.07469	14.83741
4	0.95548	13.74927
5	0.72862	10.41908
6	0.57338	19.09369
8	0.51332	15.98955

Material Properties Data: Control-Xylene

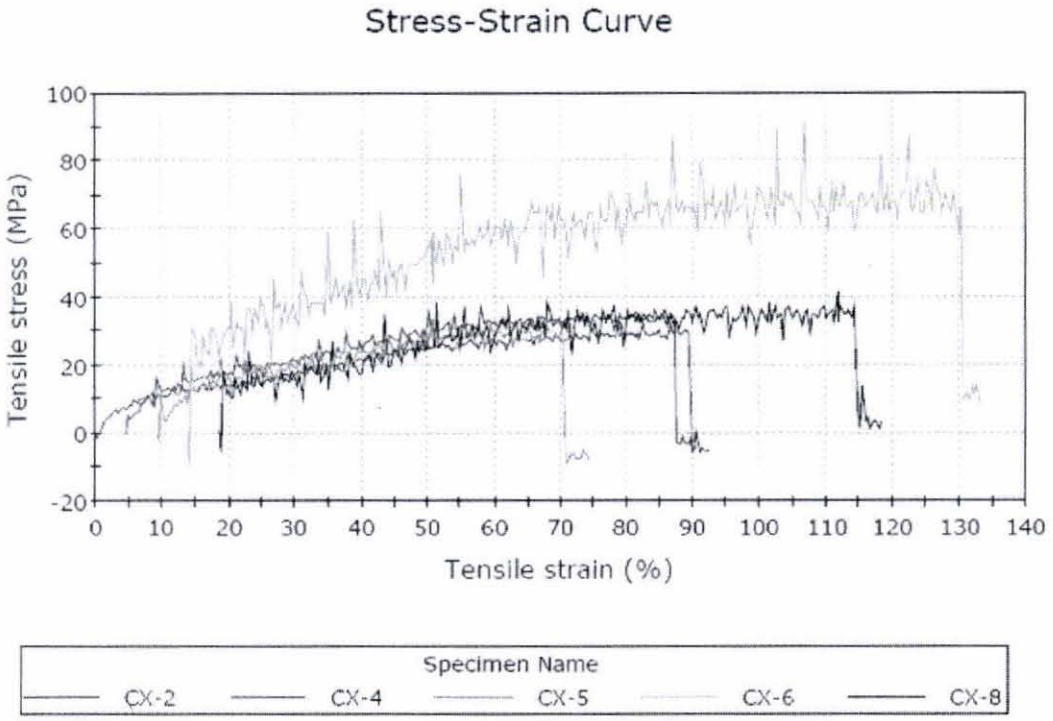

Figure C.4: Stress-strain curve for control-xylene samples.

Table C.4: Control-xylene sample material properties data.

Property Values

	Tensile stress at Tensile Strength (MPa)	Tensile strain at Break (Standard) (mm/mm)	Modulus (Young's 0 mm - 10 mm) (MPa)
2	28.38804	0.92734	101.77562
4	32.70880	0.85933	127.39238
5	29.73166	0.65119	147.84274
6	68.34279	1.19336	195.72145
8	34.37767	0.99935	80.88676

RawData: Functionalized SWNT, 0.05% wt

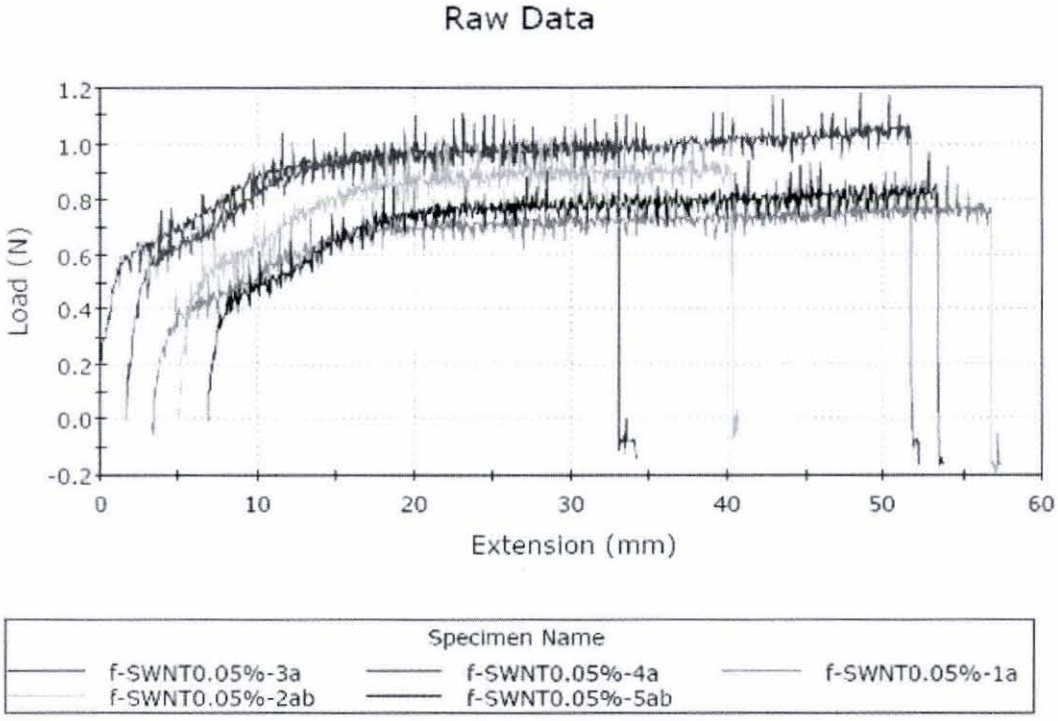

Figure C.5: Load-extension curve for f-SWNT-0.05% sample.

Table C.5: f-SWNT-0.05% sample raw data

Raw Data

	Load at Machine Peak Load (N)	Extension at Break (Standard) (mm)
7	1.11072	34.03829
8	1.18234	50.61433
10	0.91945	54.00421
11	1.02709	35.69436
12	0.97905	47.02937

Material Properties Data: Functionalized SWNT, 0.05% wt.

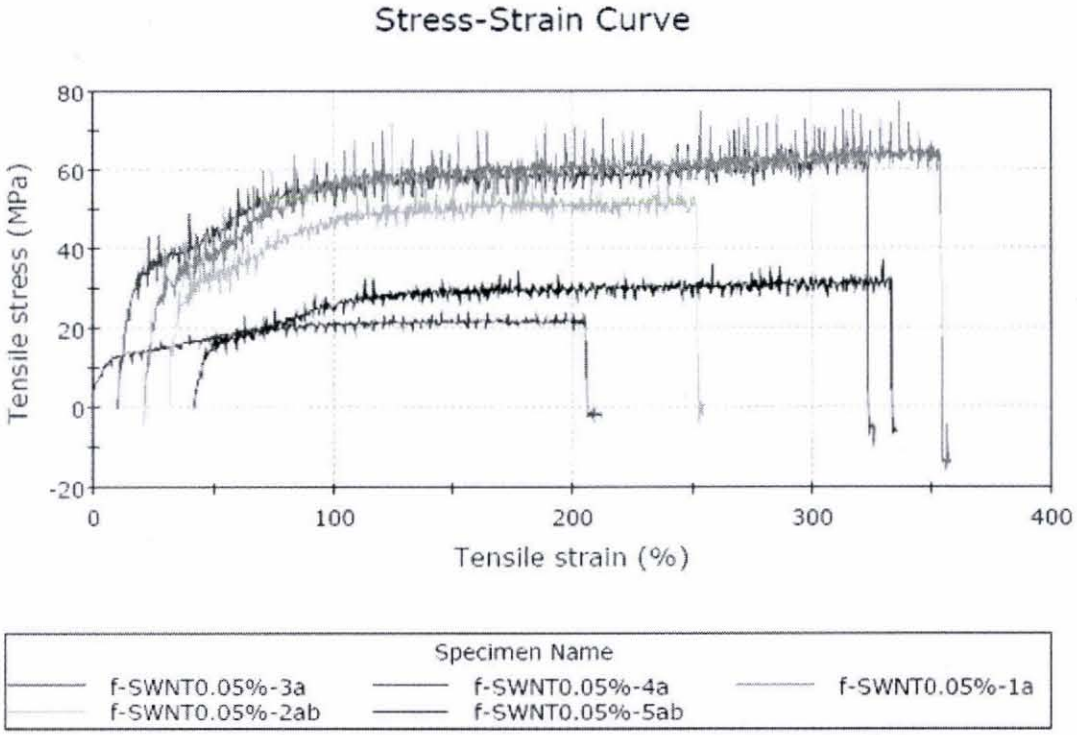

Figure C.6: Stress-strain curve for f-SWNT-0.05% samples.

Table C.6: f-SWNT-0.05% sample material properties data.

Property Values

	Tensile stress at Tensile Strength (MPa)	Tensile strain at Break (Standard) (mm/mm)	Modulus (Young's 0 mm - 10 mm) (MPa)
7	21.28568	2.12739	97.56374
8	61.34507	3.16340	296.95049
10	63.16400	3.37526	304.21626
11	50.97101	2.23090	230.79949
12	30.44358	2.93934	139.09181

Raw Data: SWNT, 0.05% wt.

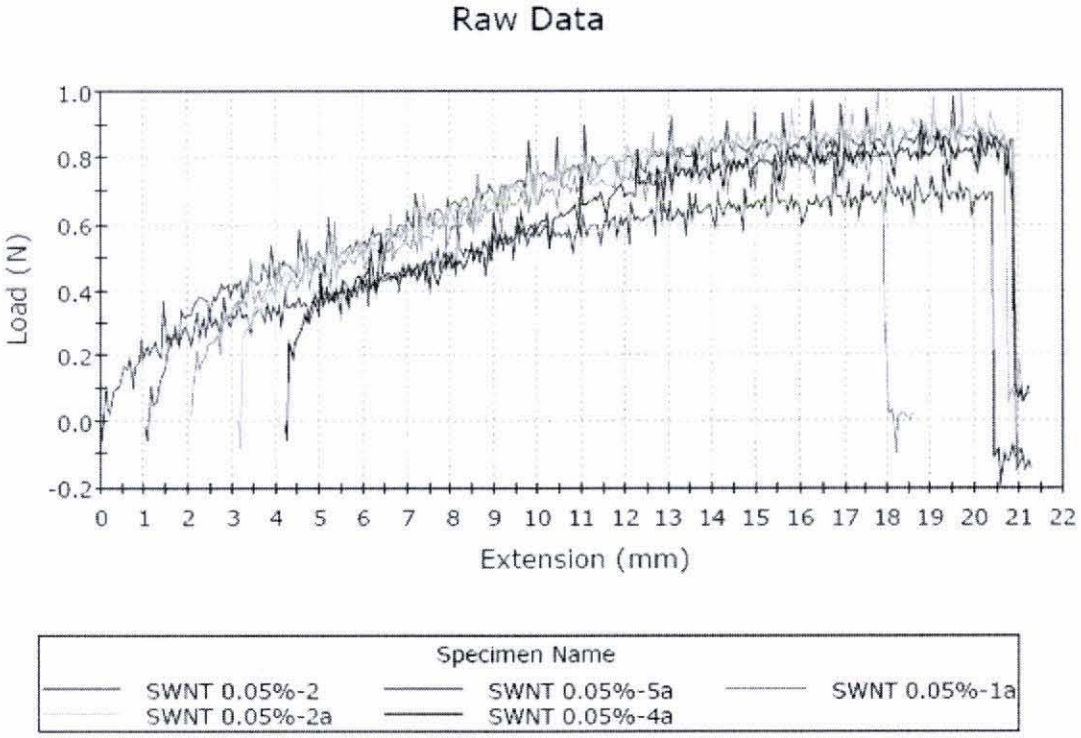

Figure C.7: Load-extension curve for SWNT-0.05% sample.

Table C.7: SWNT-0.05% sample raw data.

Raw Data

	Load at Machine Peak Load (N)	Extension at Break (Standard) (mm)
2	0.80024	21.11096
6	0.97905	20.21332
7	0.91945	16.49120
8	0.99106	18.10004
10	0.95548	17.01343

Material Properties Data: SWNT, 0.05% wt.

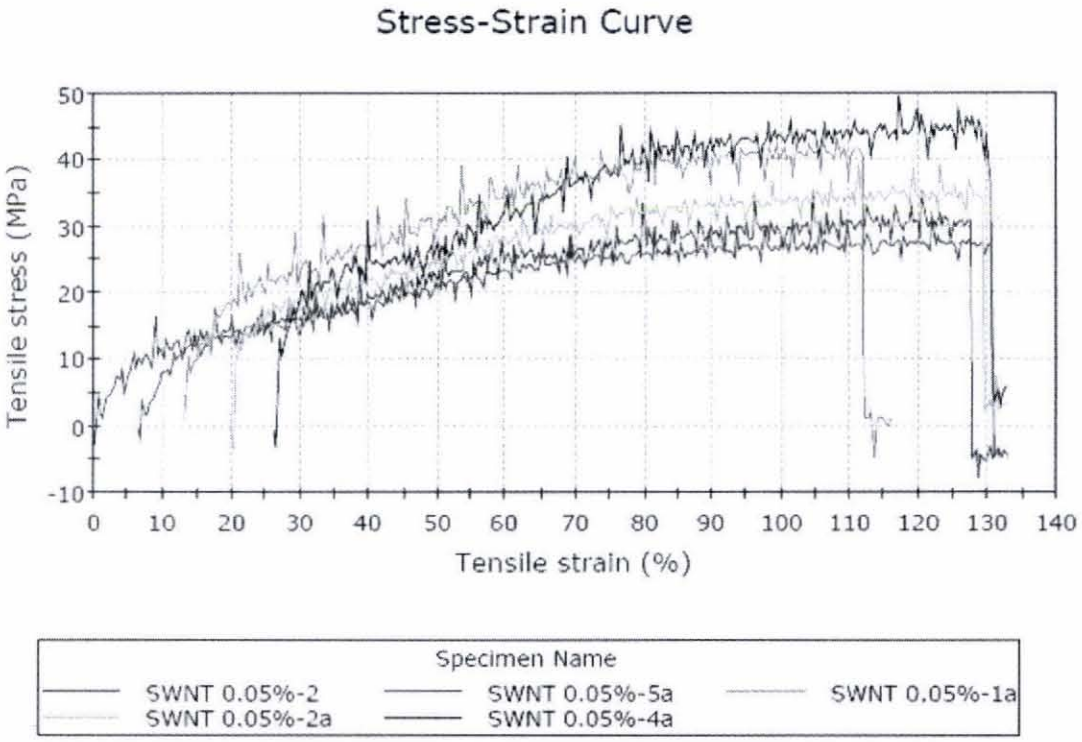

Figure C.8: Stress-strain curve for SWNT-0.05% samples.

Table C.8: SWNT-0.05% sample material properties data.

Property Values

	Tensile stress at Tensile Strength (MPa)	Tensile strain at Break (Standard) (mm/mm)	Modulus (Young's 0 mm - 10 mm) (MPa)
2	31.43728	1.31943	112.49302
6	27.53851	1.26333	126.97720
7	42.78007	1.03070	156.42524
8	34.88509	1.13125	133.18431
10	47.71308	1.06334	166.35533

Raw Data: SWNT, 0.5% wt.

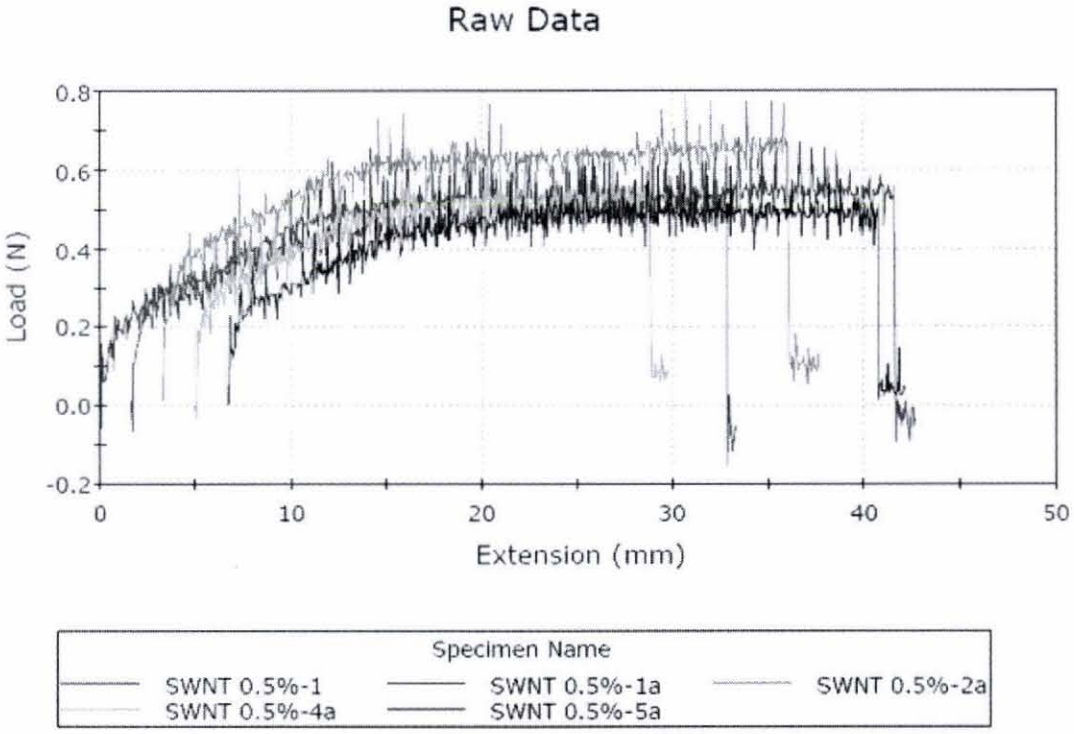

Figure C.9: Load-extension curve for SWNT-0.5% sample.

Table C.9: SWNT-0.5% sample raw data

Raw Data

	Load at Machine Peak Load (N)	Extension at Break (Standard) (mm)
1	0.65656	33.33598
6	0.69259	41.07713
7	0.81180	34.29584
9	0.66857	24.82139
10	0.63298	35.51047

Material Properties Data: SWNT, 0.5% wt.

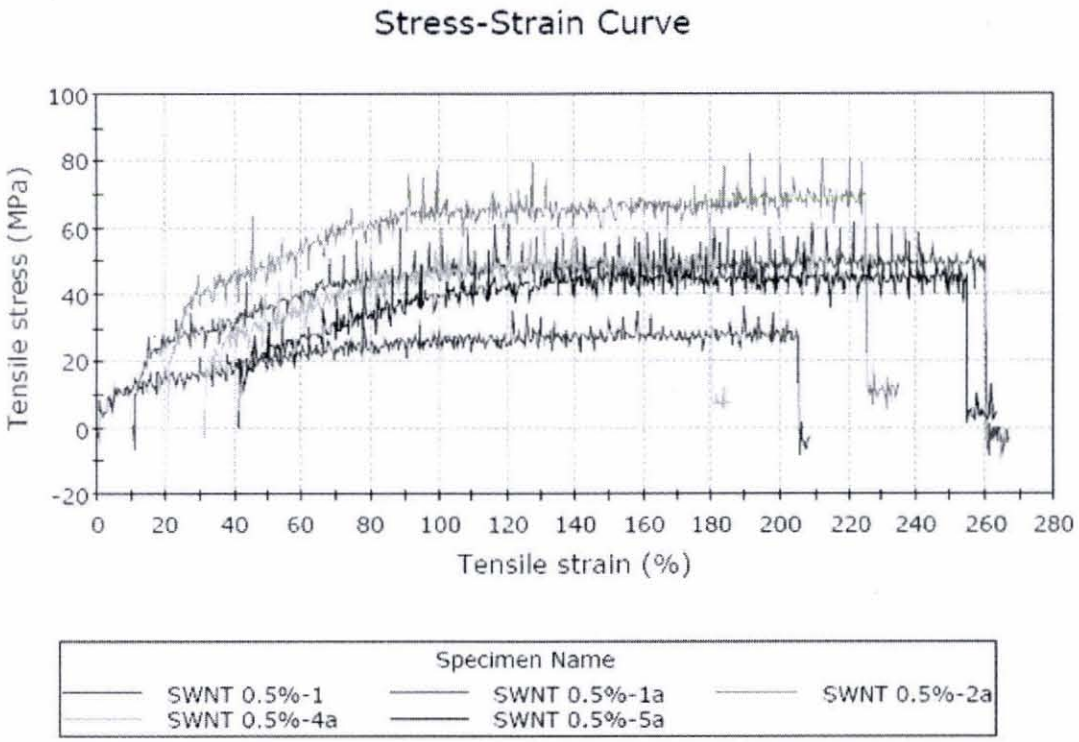

Figure C.10: Stress-strain curve for SWNT-0.5% samples.

Table C.10: SWNT-0.5% sample material properties data.

Property Values

	Tensile stress at Tensile Strength (MPa)	Tensile strain at Break (Standard) (mm/mm)	Modulus (Young's 0 mm - 10 mm) (MPa)
1	25.98685	2.08350	103.05642
6	59.64900	2.56732	216.62497
7	71.04619	2.14349	266.64986
9	49.28513	1.55134	203.25941
10	43.50183	2.21940	168.79887

Raw Data: Cadmium Sulfide Nanoparticles, 0.05% wt.

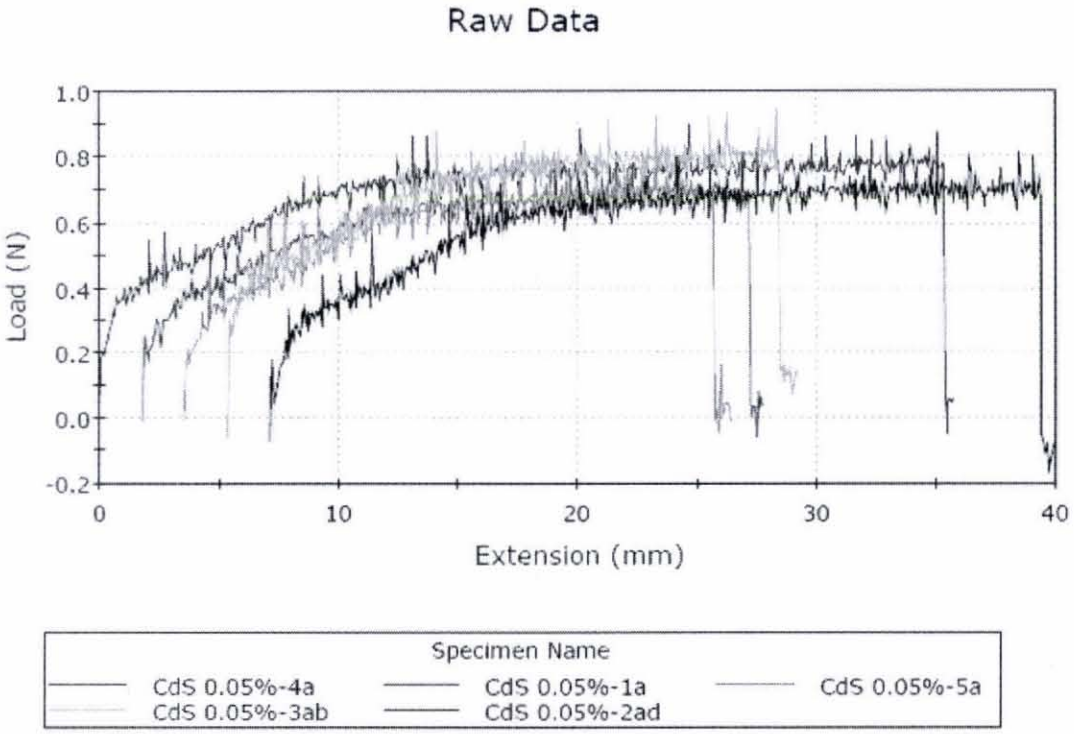

Figure C.11: Load-extension curve for CdS-0.05% sample.

Table C.11: CdS-0.05% sample raw data

Raw Data

	Load at Machine Peak Load (N)	Extension at Break (Standard) (mm)
6	0.91945	35.76396
7	0.81180	25.97201
10	0.82381	22.84019
12	0.94347	23.85212
14	0.87185	32.80943

Material Properties Data:

Cadmium Sulfide Nanoparticles, 0.05% wt.

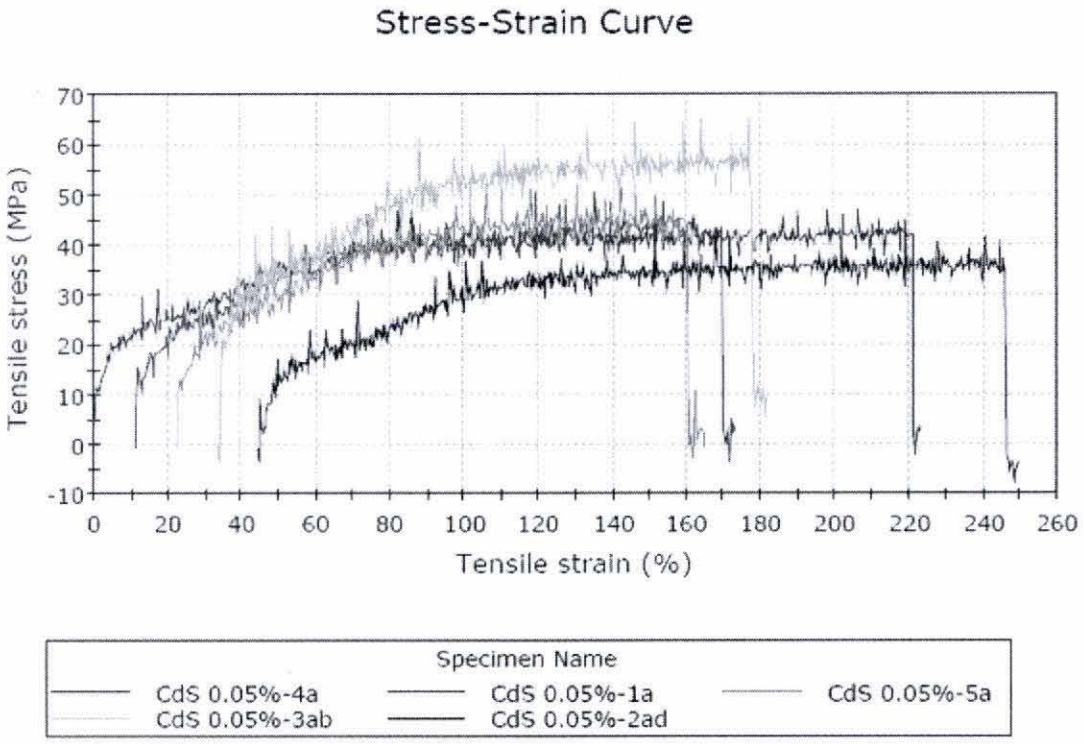

Figure C.12: Stress-strain curve for CdS-0.05% samples.

Table C.12: CdS-0.05% sample material properties data.

Property Values

	Tensile stress at Tensile Strength (MPa)	Tensile strain at Break (Standard) (mm/mm)	Modulus (Young's 0 mm - 10 mm) (MPa)
6	40.79627	2.23525	151.90079
7	43.81277	1.62325	135.03402
10	43.50691	1.42751	143.18406
12	58.53399	1.49076	209.44182
14	32.40620	2.05059	151.52384

Raw Data: Cadmium Sulfide Nanoparticles, 0.5% wt.

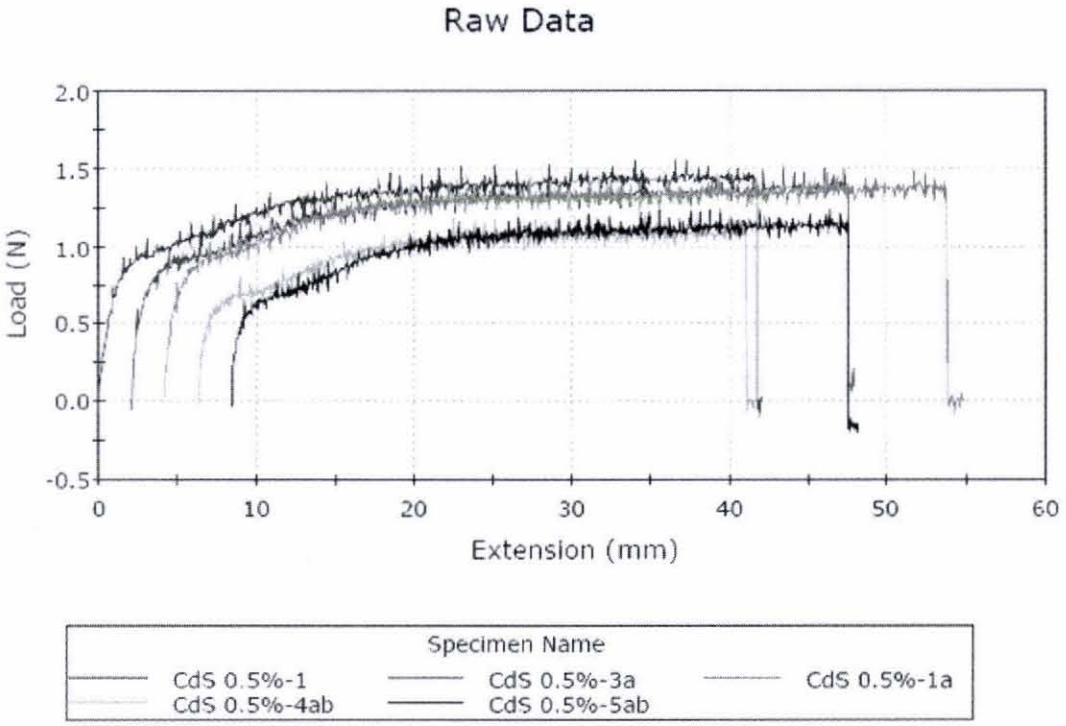

Figure C.13: Load-extension curve for CdS-0.5% sample.

Table C.13: CdS-0.5% sample raw data

Raw Data

	Load at Machine Peak Load (N)	Extension at Break (Standard) (mm)
1	1.55243	42.03700
8	1.52841	45.87723
9	1.49282	50.67986
11	1.20591	35.25368
12	1.24194	39.86251

Material Properties Data:

Cadmium Sulfide Nanoparticles, 0.5% wt.

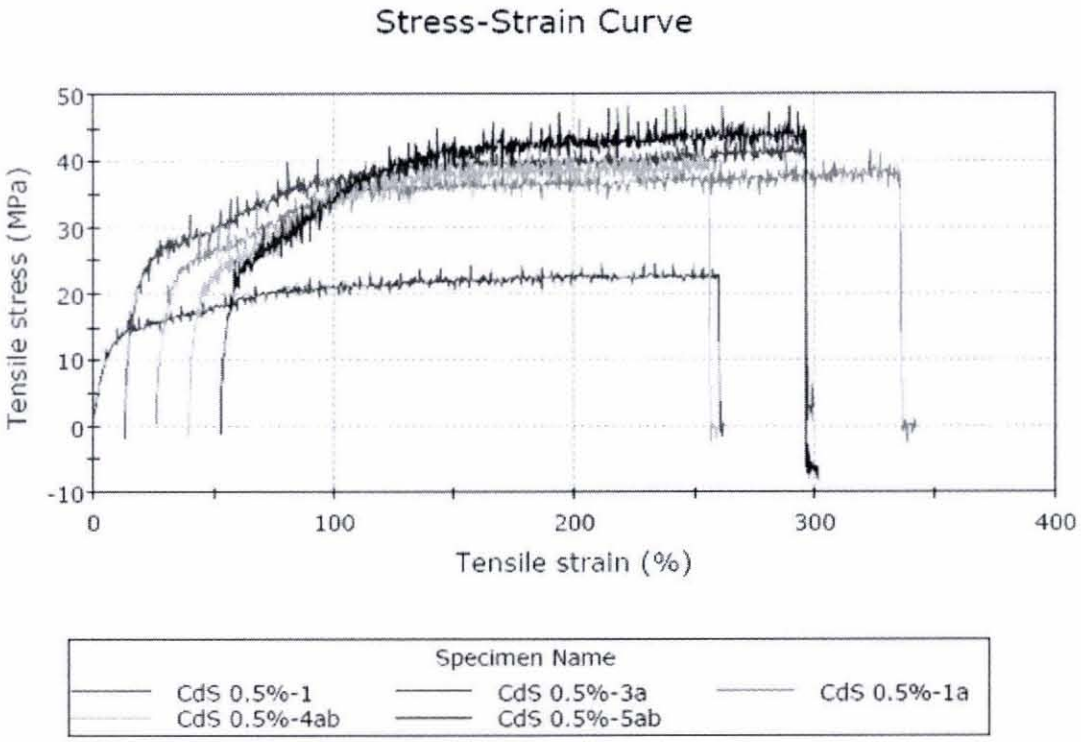

Figure C.14: Stress-strain curve for CdS-0.5% samples.

Table C.14: CdS-0.5% sample material properties data.

Property Values

	Tensile stress at Tensile Strength (MPa)	Tensile strain at Break (Standard) (mm/mm)	Modulus (Young's 0 mm - 10 mm) (MPa)
1	22.46616	2.62731	132.69294
8	41.26368	2.86733	199.69175
9	38.14598	3.16749	188.40946
11	39.01817	2.20335	181.13344
12	44.55310	2.49141	198.47377

REFERENCES

1. Yang, B., K.P. Pramoda, G.Q. Xu, and S.H. Goh, "Mechanical Reinforcement of Polyethylene Using Polyethylene-Grafted Multiwalled Carbon Nanotubes," *Advanced Functional Materials*, 2007;17(13):2062-2069.

2. Gorrasi, G., M. Sarano, A.D. Bartolomeo, D. Sannino, P. Ciambelli, and V. Vittoria, "Incorporation of Carbon Nanotubes into Polyethylene by High Energy Ball Milling: Morphology and Physical Properties," *Journal of Polymer Science: Part B*, 2007;45(5):597-606.

3. Shofner, M.L., V.N. Khabashesku, and E.V. Barrera, "Processing and Mechanical Properties of Fluorinated Single-Wall Carbon Nanotube-Polyethylene Composites," *Chemistry of Materials*, 2006;18(4):906-913.

4. Wenzhong, T., M.H. Santare, and S.G. Advani, "Melt Processing and Mechanical Property Characterization of Multi-Walled Carbon Nanotube/High Density Polyethylene (MWNT/HDPE) Composite Films," *Carbon*, 2003;41(14):2779-2785.

5. Mierczynska, A., M. Mayne-L'Hermite, G. Boiteux, and J.K. Jeszka, "Electrical and Mechanical Properties of Carbon Nanotube/Ultrahigh-Molecular-Weight Polyethylene Composites Prepared by a Filler Prelocalization Method," *Journal of Applied Polymer Science*, 2007;105(1):158-168.

6. Ruan, S.L., P. Gao, X.G. Yang, and T.X. Yu, "Toughening High Performance Ultrahigh Molecular Weight Polyethylene using Multiwalled Carbon Nanotubes," *Polymer*, 2003; 44(19):5643-5654.

7. Uehara, h., K. Kato, m. Kakiage, T. Yamanobe, and T. Komoto, "Single-Walled Carbon Nanotube Nucleated Solution-Crystallization of Polyethylene," *Journal of Physical Chemistry C*, 2007;111(51):18950-18957.

8. Liu, T., I.Y. Phang, L. Shen, S.Y. Chow, and W Zhang, "Morphology and Mechanical Properties of Multiwalled Carbon Nanotubes Reinforced Nylon-6 Composites," *Macromolecules*, 2004;37(19):7214-7222.

9. Shaffer, M.S.P., A.H. Windle, "Fabrication and Characterization of Carbon Nanotube/Poly(vinyl alcohol) Composites," *Advanced Materials*, 1999;11(11):937-941.

10. Zhang, W.D., L. Shuen, I.Y. Phang, and T.Liu, "Carbon Nanotubes Reinforced Nylon-6 Composite Prepared by Simple Melt-Compounding," *Macromolecules*, 2004;37(2):256-259.

11. Qin, S., D. Qin, W.T. Ford, D.E. Resasco, and J.E. Herrera, "Polymer Brushes on Single-Walled Carbon Nanotubes by Atom transfer Radical Polymerization of n-Butyl Methacrylate," *Journal of the American Chemical Society*, 2004;126(1):170-176.

12. Kang, M., S.J. Myung, J. Jin, "Nylon 610 and Carbon Nanotube Composite by In Situ Interfacial Polymerization," *Polymer*, 2006;47(11):3961-3966

13. Yu, G., A. Cao, C.M. Lieber, "Large-Area Blown Bubble Films of Aligned Nanowires and Carbon Nanotubes," *Nature Nanotechnology*, 2007;2(6):372-377.

14. Moniruzzaman, M., J. Chattopadhyay, W.E. Billups, and K.I. Winey, "Tuning the Mechanical Properties of SWNT/Nylon 6,10 Composites with Flexible Spacers at the Interface," *Nano Letters*, 2007;7(5):1178-1185.

15. Gao, J., M.E. Itkis, A. Yu, E. Bekyarova, B. Zhao, and R. C. Haddon, "Continuous Spinning of a Single-Walled Carbon Nanotube-Nylon Composite Fiber," *Journal of the American Chemical Society*, 2005;127(11):3847-3854.

16. Koerner, H., G. Price, N.A. Pearce, M. Alexander, and R.A. Vaia, "Remotely Actuated Polymer Nanocomposites-Stress-Recovery of Carbon-Nanotube-Filled Thermoplastic Elastomers," *Nature Materials*, 2004;3(2):115-120.

17. Kam, N.W.S., M. O'Connell, J.A. Wisdom, and H. Dai, "Carbon Nanotubes as Multifunctional Biological Transporters and Near-Infrared Agents for Selective Cancer Cell Destruction," *Proceedings of the National Academy of Sciences of the United States of America*, 2005;102;(33):11600-11605.

18. Pabba, S., A.N. Sidorov, S.M. Berry, M.M. Yazdanpanah, R.S. Keynton, G.U. Sumanasekera, and R.W. Cohn, "Oriented Nanomaterial Air Bridges

Formed from Suspended Polymer-Composite Nanofibers," *American Chemical Society Nano*, 2007;1(1):57-62.

19. Surani, F.B., X. Kong, D.B. Panchal, and Y. Qiao, "Energy Absorption of a Nanoporous System Subjected to Dynamic Loadings," *Applied Physics Letters*, 2005;87(16):163111-1-163111-3.

20. Wang, Z.L. and J. Song, "Piezoelectric Nanogenerators Based on Zinc Oxide Nanowire Arrays," *Science*, 2006(5771);312:242-246.

21. Han, J., A. Globus, R. Jaffe, and G. Deardorff, "Molecular Dynamics Simulations of Carbon Nanotube-Based Gears," *Nanotechnology*, 1997;8(3):95-102.

22. Murakami, H. and N. Nakashima, "Soluble Carbon Nanotubes and their Applications," *Journal of Nanoscience and Nanotechnology*, 2006;6(1):16-27.

23. Baughman, R.H., A. Zakhidov, and W.A. de Heer, "Carbon Nanotubes-the Route Toward Applications," *Science*, 2002; 297(5582):787-792.

24. Williams, David J. *Polymer Science and Engineering*, New Jersey: Prentice-Hall; 1971.

25. Stevens, Malcom P. *Polymer Chemistry, An Introduction, 2nd ed.* New York: Oxford University Press; 1990.

26. Iijima, S., "Helical Microtubules of Graphitic Carbon," *Nature*, 1991;354(6348):56-58.

27. Ajayan, P.M. "Carbon Nanotubes." Hari Singh Nalwa, ed. *Nanostructured Materials and Nanotechnology*. San Diego: Academic Press; 2002: 329-360.

28. Cao, A., P.L. Dickrell, W.G. Sawyer, M.N. Ghasemi-Nejhad, and P.M. Ajayan, "Super-Compressible Foamlike Carbon Nanotube Films," *Science*, 2005;310(5752):1307-1310.

29. Falvo, M.R., G.J. Clary, R.M. Taylor II, V. Chi, F.P. Brooks Jr., S. Washburn, and R. Superfine, "Bending and Buckling of Carbon Nanotubes Under Large Strain," *Nature*, 1997;389(6651):582-584.

30. Daraio, C., V.F. Nesterenko, and S. Jin, "Impact Response by Foamlike Forest of Coiled Carbon Nanotubes," *Journal of Applied Physics*, 2006;100(6):064309-1-064309-4.

31. Deck, C.P., J. Flowers, G.S.B. Mckee, and D. Vecchio, "Mechanical Behavior of Ultralong Multiwalled Carbon Nanotube Mats," *Journal of Applied Physics*, 2007;101(2):023512-1-023512-9.

32. Yu, M., B.S. Files, S. Arepalli, and R.S. Ruoff, "Tensile Loading of Ropes of Single Wall Carbon Nanotubes and their Mechanical Properties," *Physical Review Letters*, 2000;84(24):5552-5555.

33. Zhang, X., T.V. Sreekumar, T. Liu, and S. Kumar, "Properties and Structure of Nitric Acid Oxidized Single Wall Carbon Nanotube Films," *Journal of Physical Chemistry B*, 2004;108(5):16435-16440.

34. Chen, J., A.M. Rao, S. Lyuksyutov, M.E. Itkis, M.A. Hamon, H. Hu, R.W. Cohn, P.C. Eklund, D.T. Colbert, R.E. Smalley, and R.C. Haddon, "Dissolution of Full-Length Single-Walled Carbon Nanotubes," *Journal of Physical Chemistry B*, 2001;105(13):2525-2528.

35. Liu, J., A.G. Rinzler, H. Dai, J.H. Hafner, R.K. Bradley, P.J. Boul, A. Lu, T. Iverson, K. Shelimov, C.B. Huffman, F Rodriguez-Macias, Y.S. Shon, T.R. Lee, D.T. Colbert, and R.E. Smalley, "Fullerene Pipes," *Science*, 1998;280(5367):1253-1255.

36. Dyke, C.A. and J.M. Tour, "Solvent-Free Functionalization of Carbon Nanotubes," *Journal of the American Chemical Society*, 2003;125(5):1156-1157.

37. Pompeo, F. and D.E. Resasco, "Water Solubilization of Single-Walled Carbon Nanotubes by Functionalization with Glucosamine," *Nano Letters*, 2002;2(4):369-373.

38. Salvetat, J.P., G.A.D. Briggs, J.M. Bonard, R.R. Bacsa, A.J. Kulik, T. Stockli, N.A. Burnham, and L. Forro, "Elastic and Shear Moduli of Single-Walled Carbon Nanotube Ropes," *Physical Review Letters*, 1999;82(5):944-947.

39. Zhang, M., K.R. Atkinson, and R.H. Baughman, "Multifunctional Carbon Nanotube Yarns by Downsizing and Ancient Technology," *Science*, 2004;306(5700):1358-1361.

40. Jiang, K., Q. Li, and S. Fan, "Spinning Continuous Carbon Nanotube Yarns," *Nature*, 2002;419(6909):801.

41. Zhang, M. S. Fang, A. A. Zakhidov, S.B.Lee, A.E. Aliev, C.D. Williams, K.R. Atkinson, and R.H. Baughman, "Strong, transparent, Multifunctional, Carbon Nanotube Sheets," *Science*, 2005;309(5738):1215-1219.

42. Mansoori, G. Ali. *Principles of Nanotechnology*. Singapore: World Scientific, 2005.

43. Koruga, D., S. Hameroff, J. Withers, R. Loutfy, and M. Sundareshan. *Fullerene C_{60} History, Physics, Nanobiology, Nanotechnology*, North-Holland: Elsevier Science; 1993.

44. Hearle, J.W.S., P. Grosberg, S. Backer. *Structural Mechanics of Fibers, Yarns, and Fabrics*. New York: Wiley-Interscience; 1969.

45. Jang, B.Z., Y.K. Lieu, Y.S. Chang, and L.R. Hwang, "Cryogenic Failure Mechanisms of Fiber-Epoxy Composites for Energy Applications," *Polymer Composites*, 1987;8(3):188-198.

46. Knapp, R.H., "Derivation of a New Stiffness Matrix for Helically Armoured Cables Considering Tension and Torsion," *International Journal for Numerical Methods in Engineering*, 1979;14(4):515-529.

47. Yu, M., T. Kowalewski, and R.S. Ruoff, "Structural Analysis of Collapsed, and Twisted and Collapsed, Multiwalled Carbon Nanotubes by Atomic Force Microscopy," *Physical Review Letters*, 2001;86(1):87-90

48. Williams, P.A., S.J. Papadakis, A.M. Patel, M.R. Falvo, S. Washburn, and R. Superfine, "Torsional Response and Stiffening of Individual Multiwalled Carbon Nanotubes," *Physical Review Letters*, 2002;89(25):255502-1-255502-4.

49. Ando, Y., X. Zaho, T. Sugai, M. Kumar, "Growing Carbon Nanotubes," *Materials Today*, 2004;7(10):22-29.

50. Endo, M., T. Hayashi, Y.A. Kim, and H. Muramatsu, "Development and Application of Carbon Nanotubes," *Japanese Journal of Applied Physics*, 2006;45(6A):4883-4892.

51. Sinnott, S.B., R. Andrews, D.Qian, A.M. Rao, Z. Mao, E.C. Dickey, and F. Derbyshire, "Model of Carbon Nanotube Growth through Chemical Vapor Deposition," *Chemical Physics Letters*, 1999;315(1):25-30.

52. ASTM standard: D3822, Standard Test Method for Tensile Properties of Single Textile Fibers, 2007;07.01,904-913

53. Gere, James M. *Mechanics of Materials, 5th ed.* Pacific Grove, CA: Brooks/Cole; 2001.